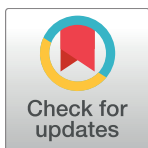


RESEARCH ARTICLE

# A model of the onset of the senescence associated secretory phenotype after DNA damage induced senescence

Patrick Meyer<sup>1,2\*</sup>, Pallab Maity<sup>1,2\*</sup>, Andre Burkovski<sup>3,4</sup>, Julian Schwab<sup>3,4</sup>, Christoph Müssel<sup>3</sup>, Karmveer Singh<sup>1,2</sup>, Filipa F. Ferreira<sup>1</sup>, Linda Krug<sup>1,2</sup>, Harald J. Maier<sup>2</sup>, Meinhard Wlaschek<sup>1,2</sup>, Thomas Wirth<sup>5</sup>, Hans A. Kestler<sup>2,3,4†\*</sup>, Karin Scharffetter-Kochanek<sup>1,2</sup>‡



**1** Department of Dermatology and Allergic Diseases, University of Ulm, Germany, **2** Aging Research Center (ARC), University of Ulm, Germany, **3** Institute of Medical Systems Biology, University of Ulm, Germany, **4** International Graduate School in Molecular Medicine, University of Ulm, Germany, **5** Institute of Physiological Chemistry, University of Ulm, Germany

\* These authors contributed equally to this work.

† These authors are joint senior authors on this work.

\* [hans.kestler@uni-ulm.de](mailto:hans.kestler@uni-ulm.de)

## OPEN ACCESS

**Citation:** Meyer P, Maity P, Burkovski A, Schwab J, Müssel C, Singh K, et al. (2017) A model of the onset of the senescence associated secretory phenotype after DNA damage induced senescence. PLoS Comput Biol 13(12): e1005741. <https://doi.org/10.1371/journal.pcbi.1005741>

**Editor:** Paola Vera-Licona, University of Connecticut Health Center, UNITED STATES

**Received:** November 28, 2016

**Accepted:** August 22, 2017

**Published:** December 4, 2017

**Copyright:** © 2017 Meyer et al. This is an open access article distributed under the terms of the [Creative Commons Attribution License](#), which permits unrestricted use, distribution, and reproduction in any medium, provided the original author and source are credited.

**Data Availability Statement:** All relevant data are within the paper and its Supporting Information files. This plasmid (pCAG-Cre-T2A-mRuby2) can be obtained from the authors on request and was deposited in the Addgene repository (Accession ID 102989).

**Funding:** KS-K is supported by the German Research Foundation (DFG, SCHA411/15-2) within the Clinical Research Group KFO142 “Cellular and Molecular Mechanisms of Ageing – From Mechanisms to Clinical Perspectives”, also by the

## Abstract

Cells and tissues are exposed to stress from numerous sources. Senescence is a protective mechanism that prevents malignant tissue changes and constitutes a fundamental mechanism of aging. It can be accompanied by a senescence associated secretory phenotype (SASP) that causes chronic inflammation. We present a Boolean network model-based gene regulatory network of the SASP, incorporating published gene interaction data. The simulation results describe current biological knowledge. The model predicts different *in-silico* knockouts that prevent key SASP-mediators, IL-6 and IL-8, from getting activated upon DNA damage. The NF-κB Essential Modulator (NEMO) was the most promising *in-silico* knockout candidate and we were able to show its importance in the inhibition of IL-6 and IL-8 following DNA-damage in murine dermal fibroblasts *in-vitro*. We strengthen the speculated regulator function of the NF-κB signaling pathway in the onset and maintenance of the SASP using *in-silico* and *in-vitro* approaches. We were able to mechanistically show, that DNA damage mediated SASP triggering of IL-6 and IL-8 is mainly relayed through NF-κB, giving access to possible therapy targets for SASP-accompanied diseases.

## Author summary

The senescence associated secretory phenotype is developed by cells undergoing permanent cell cycle arrest. This phenotype is characterized by the secretion of a variety of factors that facilitate tissue breakdown and inflammation and is therefore theorized to, in part, be causal for aging and age-related diseases. In recent years the SASP has been implicated in a variety of chronic inflammatory diseases. Due to these advances, it is imperative to better understand the dynamics of this cellular phenotype and to find ways to disrupt

Graduate Training Centre GRK 1789 “Cellular and Molecular Mechanisms in Ageing (CEMMA)”, and collaborative Project FKZ0315894A SyStaR - Molecular Systems Biology of Impaired Stem Cell Function and Regeneration during Aging, and Collaborative Research Centre CRC1149 Danger Response, Disturbance Factors and Regenerative Potential after Acute Trauma and the Förderlinie Perspektivförderung “Zelluläre Entscheidungs- und Signalwege bei der Alterung” of the Ministerium für Wissenschaft, Forschung und Kunst Baden-Württemberg, Germany. HAK is supported by the European Community’s Seventh Framework Programme (FP7/2007–2013) under grant agreement n602783, the DFG (SFB 1074 project Z1), and the German Federal Ministry of Education and Research (BMBF, Gerontosys II, Forschungskern SyStaR, project ID 0315894A and e.Med, SYMBOL-HF, ID 01ZX1407A)

**Competing interests:** The authors have declared that no competing interests exist.

it. We have developed a Boolean network incorporating the major signaling pathways of the SASP that allows us to specifically investigate interactions of the pathways and genes involved. We validated our model by reliably reproducing published data on the SASP. We utilized our model to uncover components that directly control the detrimental effects of the senescence associated secretory phenotype that are largely caused by IL-6 and IL-8, two major factors of the SASP in establishing and spreading senescence as well as causing local inflammation. In subsequent in-vitro experiments, we were able to verify our computational results and could suggest NEMO as one potential target for therapy of SASP-related diseases.

## Introduction

Age-related diseases can be held accountable for the major part of morbidity and mortality in an ageing population. Additionally they cause a large proportion of yearly health costs [1]. Cellular senescence is one of the most prominent events that is likely to contribute to ageing. It refers to the irreversible cell cycle arrest that is essential when cells encounter detrimental changes. Once in permanent arrest, these cells are normally cleared by the immune system before they are able to do any harm to the organism [2]. However, some of these cells persist and develop a secretory phenotype releasing a variety of factors among which pro-inflammatory cytokines, chemokines and extracellular matrix degrading proteases are included. Together these shape the senescent-associated secretory phenotype or SASP [3–5].

While the SASP can cause chronic inflammation in tissue, it can also reinforce senescence in autocrine and paracrine manner [6, 7]. This feature of the SASP not only keeps senescent cells in their growth arrested states but it promotes senescence spreading to healthy bystander cells. Therefore, the SASP contributes to the accumulation of senescent cells during ageing, but also supports the emergence of age-related chronic diseases and tissue dysfunctions by elevating inflammatory processes [6, 8]. Major soluble factors that facilitate this bystander-infection of healthy cells are IL-6 and IL-8. Both have been shown to be important in the maintenance and spreading of oncogene- and DNA-damage-induced senescence [3]. Also, both have been shown to be highly overexpressed by senescent cells and are known to locally and systemically play important roles in the regulations of a variety of processes in the aging body [3, 4, 9]. IL-6, in fact, most likely contributes to organ dysfunction during aging thus promoting frailty [8].

To allow for a deeper understanding of the SASP and the dynamics of its complex interactions a computational model of the Regulatory Network (RN) [10] and subsequent simulations can be insightful. RNs can be described by different mathematical models such as differential equations, Bayesian networks, and Boolean networks among others [11]. The Boolean network model [12, 13], as opposed to other model approaches, can be based on qualitative knowledge only. In gene-gene interaction, for example, the expression of a gene is regulated by transcription factors binding to its regulatory regions. The activation of a gene follows a switch-like behavior depending on the concentration of its transcription factors. This behavior allows common approximation of the possible states of a gene to be active or inactive [14, 15]. Ultimately, this can be encoded as Boolean logical values: true (“1”) or false (“0”). The interactions between genes, e.g. whether a factor acts as an activator, repressor or both can be described by functions. These Boolean functions are the basis to simulate dynamic behavior, i.e. changes over time. As every regulatory factor has two possible states (active or inactive) in a Boolean network model,  $2^x$  possible state combinations (i.e. gene activation patterns) exist for  $x$  genes.

For any activation pattern, iterative updates of genes in the network through consecutive application of the Boolean rules eventually lead to sequences of gene activation patterns that are time-invariant, called attractors. These attractors can correspond to observed expression profiles of biological phenotypes or can be used to create hypotheses to further evaluate in wet-lab experiments [16, 17]. Different update strategies for the Boolean functions exist. Using a synchronous update strategy means applying all Boolean functions simultaneously, also assuming that regulatory factors interact independently of one another and that their interaction has a similar time scale resolution. Relaxing these assumptions leads to the concept of asynchronous updates where each Boolean function is updated separately one at a time in any order. This allows a more direct modelling of different time scales. The asynchronous update strategy also usually generates trajectories that are different from those of synchronous Boolean networks. The state transition graph of an asynchronous Boolean network becomes a Markov chain which requires the additional definition of transition probabilities in each node of the state graph. Interestingly, point attractors (those with one state) in asynchronous Boolean networks are the same as those in synchronous Boolean networks. However, these networks can also show loose/complex attractors [18] which are part of active research [19, 20]. Another extension of Boolean networks are probabilistic Boolean networks, which may define more than one Boolean function for regulatory factors where each function has a specific probability to be chosen for update. Although this concept may closer represent a biological system, it again requires parameter estimation for the probabilities. However, estimation of the probabilities naturally demands large amounts of interaction specific data which is, for larger networks, neither economically, nor experimentally viable. In our case, we decided to focus on synchronous Boolean networks, partly due to their proven usability, and their ability to reveal key dynamical patterns of the modelled system. However, to strengthen our models' hypothesis, we additionally performed *in-silico* experiments with an asynchronous update scheme (S1 Text).

Synchronous Boolean networks have been used to model the oncogenic pathways in neuroblastoma [21], the *hrp* regulon of *Pseudomonas syringae* [22], the blood development from mesoderm to blood [23], the determination of the first or second heart field identity [24] as well as for the modeling of the Wnt pathway [25]. The qualitative knowledge base that is necessary to reconstruct [26] a Boolean network model consists mostly of reports on specific interactions that describe local regulation of genes or proteins. Boolean network models utilize this knowledge about local regulations to reconstruct a first global mechanistic model of SASP. In summary, such a model allows to generate hypotheses about regulatory influences on different local interactions. These interactions, in turn, can be tested in wet-lab in order to validate the generated hypothesis and assess the accuracy of the proposed model.

Here, we present a regulatory Boolean network of the development and maintenance of senescence and the SASP incorporating published gene interaction data of SASP-associated signaling pathways like IL-1, IL-6, p53 and NF- $\kappa$ B. We simulated the model and retrieved steady states of pathway interactions between p53/p16<sup>INK4A</sup> steered senescence, IL-1/IL-6 driven inflammatory activity and the emergence and retention of the SASP through NF- $\kappa$ B and its targets. This Boolean network enables the highlighting of key players in these processes. Simulations of knock-out experiments within this model go in line with previously published data. The subsequent validation of generated *in-silico* results *in-vitro* was done in murine dermal fibroblasts (MDF) isolated from a murine NF- $\kappa$ B Essential Modulator (NEMO)-knockout system in which DNA damage was introduced. The NEMO knockout inhibits IL-6 and IL-8 homologue mRNA expression and protein secretion in MDFs after DNA damage *in-vitro*, possibly enabling at least a lowering of the contagiousness for neighboring cells and the protumorigenic potential of the SASP. The model presented in this article allows a mechanistic view on interaction between the proinflammatory and DNA-damage signaling pathways and

thereby helps to gain insights into the dynamics of the SASP. Furthermore, it enables to generate extensive hypotheses about possible knockout targets that can be experimentally tested and verified *in-vitro*. To the best of our knowledge, this report is the first one that combined *in-silico* simulation of the SASP with its laboratory based experimental validation.

## Results

### The network model exhibits stable states for cell cycle progression and senescence

The reconstruction of a Boolean network model for SASP requires screening for many candidate interactions in published literature and data. Although the model, after reconstruction, may be reduced in the number of components [20, 27, 28], it would potentially hide some of the interaction targets and regulatory factors with regard to the signaling cascade. The regulatory factors defined in this model are beneficial if one wants to extend the model and include additional related signaling pathways. The subsequent model must accurately correspond to the current understanding of the process at hand, i.e., able to predict well-known phenotypes of SASP. Biological phenotypes represent a long-term behavior of a biological system based on interaction of regulatory factors. In the same sense, attractors are the long-term behavior of a Boolean network model based on the Boolean rules of modelled regulatory factors. Hence, there is a natural correspondence between biological phenotypes and attractors in the Boolean network. In the following, we use figures that depict the signaling cascade towards an attractor as well as the attractor itself. The interpretation of these attractors in the context of SASP further allows generation of hypotheses that can be tested in a biological system.

The information for the reconstruction of these networks was collected from published data. An overview of the genes incorporated in this model and their interaction can be found in Fig 1. The corresponding Boolean rules are listed in Table 1. The network depicts processes following a cell cycle arrest inducing action, such as DNA damage and other cellular stresses. Here, we analyze SASP under strong DNA damage and do not distinguish between different levels of DNA damage.

We first analyzed if our model can render steady states for cell cycle progression when there is no stress signal input. Our data show a normal cell cycle progression with active CDK2 and CDK4, as well as phosphorylated Rb and hence an active E2F. No other signaling pathways that are implemented in this model were activated which can be seen as normal cell cycle progression (Fig 2).

Upon the outside signal DNA damage, we observe first the activation of the DNA damage response with a subsequent activation of p53 and p16<sup>INK4A</sup> signaling, leading to a stop in cell cycle progression and at a later time point to permanent cell cycle arrest. Simultaneously NF-κB signaling gets activated by the DNA damage response through NEMO, giving rise to beneficial but also detrimental effects of NF-κB like the senescence associated secretory phenotype (Fig 3).

After entering p53/p21 and p16<sup>INK4A</sup> mediated permanent cell cycle arrest upon DNA damage, the activation of NF-κB leads to an increase of IL-1, IL-6 as well as IL-8 expression among others [29–33]. Our model shows the direct activation of these cytokines and chemokines by NF-κB after its activation through the DNA damage response and NEMO (Fig 3).

### The Boolean network describes published knock-out and overexpression phenotypes

The NF-κB pathway has been studied extensively and there are knockout mice available for all proteins of the pathway, however some of them are embryonically lethal due to the importance

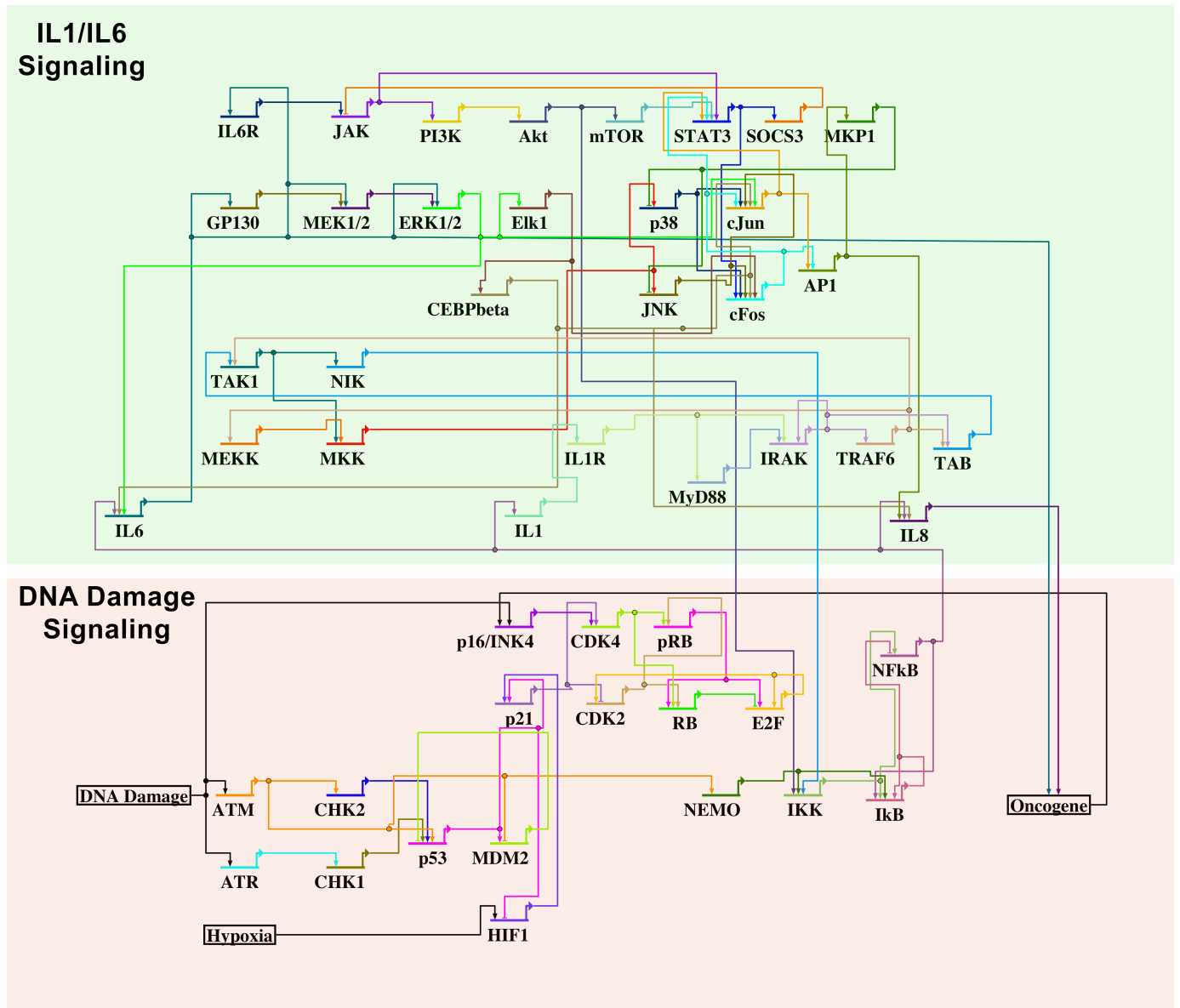


**Fig 1. Boolean network for gene regulation during cell cycle progression and the onset of cell cycle arrest after DNA damage.** The overview shows the network wiring of the known gene regulations during DNA damage with a focus on the DNA damage repair/cell cycle arrest signaling. Cell cycle arrested cells over time show a tendency to develop a secretory phenotype that causes them to secrete high amounts of proinflammatory factors that can negatively influence neighboring cells. Major signaling pathways of these factors are included in this overview and in the Boolean network. Arrows indicate gene activation and inhibition is depicted as bar head. However, the interaction may be more complex and the corresponding Boolean rules are given in Table 1.

<https://doi.org/10.1371/journal.pcbi.1005741.g001>

of NF- $\kappa$ B signaling in regulating development and apoptosis. We therefore focused on published *in-vitro* knockout and overexpression phenotypes. IL-6 and IL-8 are extremely important in maintaining and spreading the SASP in an autocrine as well as paracrine fashion. Hence, we followed the question what knockouts and/or overexpressions the Boolean network model suggests to inhibit the expression of IL-6 and IL-8 under the assumption of existing DNA damage. These simulations are included in [S1 Text](#).

**Table 1. Boolean network for gene regulation during cell cycle progression and the onset of cell cycle arrest after DNA damage.** Boolean Rules using operators “&” (logical and), “|” (logical or) and “¬” (logical not).

DNA Damage/Senescence signaling		
Regulatory Factor at time $t+1$	Boolean rule update given regulatory factor state at time $t$	
<i>DNA Damage, Defective Telomeres, etc.</i>		
DNAD	DNAD	This rule serves as an input signal to any kind of severe DNA damage.
<i>Oncogene induced senescence</i>		
Oncogene	IL8   IL6	Active IL-6 or IL-8 signaling characterize the activation of Oncogene. Moreover, IL-6 and IL-8 also required for oncogene induced senescence [3].
Hypoxia	Hypoxia	Exogenous factor describing Hypoxia.
<i>In presence of DNA damage, a cell activates regulatory factors ATR and ATM, which subsequently activate checkpoints CHK1 and CHK2.</i>		
ATM	DNAD	ATM is active in presence of DNA damage [57–59].
CHK2	ATM	ATM subsequently activates CHK2 [60].
ATR	DNAD	ATR is active in presence of DNA damage [57, 59].
CHK1	ATR	ATR subsequently activates CHK1 [61].
p53	(CHK2   CHK1   ATM) & ( $\neg$ MDM2)	p53 can be activated by any of CHK1 [62], CHK2 [62, 63] or ATM [62, 64]. However, MDM2 is a strong inhibitor of p53 [62, 65].
HIF1	Hypoxia & ( $\neg$ p53)	HIF1, which is active during Hypoxia [66], is inhibited by p53 [67].
p21	p53   HIF1	p21 is activated by p53 [68] as well as by HIF1 [69].
CDK2	E2F & ( $\neg$ p21)	CDK2 requires activation of E2F. p21 inhibits the CDK2 complex [68].
RB	$\neg$ (pRB   CDK4   CDK2)	RB, which is active in its hypophosphorylated state (RB) is hyperphosphorylated and inactivated (pRB) by CDK4 and CDK2 [70–72].
pRB	(CDK4   CDK2)	RB is phosphorylated (pRB) in presence of any cyclin dependent kinases CDK4 and CDK2 [70–72].
E2F	(pRB   E2F) & $\neg$ RB	E2F is positively autoregulated and active in presence of hyperphosphorylated RB (pRB). Active RB, however, inhibts E2F [38].
MDM2	p53 & $\neg$ ATM	p53 activates MDM2 [65, 73, 74], while ATM inhibits MDM2 [64].
p16INK4	Oncogene   DNAD	Activation of p16INK4 depends on either DNA damage or Oncogene or both [75].
CDK4	$\neg$ (p16INK4   p21)	CDK4 is inhibited by p16INK4 [75] and p21 [68].
NEMO	DNAD	NEMO is activated by DNA damage [76, 77].
IKK	NEMO   NIK   Akt	IKK can be activated by any of NEMO [78], NIK [79] or Akt [80].
IkB	(NFkB   IkB) & $\neg$ (IKK & NEMO)	IkB is activated NFkB complex or IkB itself [81]. IKK [82] and NEMO [83] together are required to inhibit IkB.
NFkB	IKK & $\neg$ IkB	NFkB is activated by IKK, while inhibited by IkB [82, 83].
<b>IL-1 signaling</b>		
IL1	NFkB	IL1 is activated by NFkB [29, 30].
IL1R	IL1	IL1 binds to and activates IL1 receptor (IL1R) [84].
MyD88	IL1R	MyD88 is an adaptor molecule in IL1-IL1R pathway and bridging IL1R to the IRAK complex IL1R [84].
IRAK	IL1R   MyD88   IRAK	IRAK is autoactivated [85, 86] and also is activated by IL1R [84, 86] and MyD88 [85, 87].
TRAF6	IRAK	TRAF6 is activated by IRAK [85].
TAB	(TRAF6   IRAK)	TAB is activated by any of TRAF6 [88, 89] or IRAK [89].
TAK1	(TRAF6   TAB)	TAK1 is activated by any of TRAF6 [88, 89] or TAB [90].
MEKK	TRAF6	MEKK is activated by TRAF6 [89].
MKK	(TAK1   MEKK)	MKK is activated by any of TAK1 [91, 92] or MEKK [93].
JNK	MKK & $\neg$ MKP1	JNK is activated by MKK [94, 95] while is inhibited by MKP1 [96].
p38	MKK & $\neg$ MKP1	p38 is activated by MKK [97] while inhibited by MKP1 [98].
cJun	(p38   JNK   ERK1_2   CEBPbeta) & cFos	cFos is required for the action of cJun and can be activated by any one of p38 [99, 100], JNK [101], ERK1_2 [102] or CEBPbeta [103].

(Continued)

**Table 1.** (Continued)

DNA Damage/Senescence signaling		
cFos	p38   JNK   Elk1   CEBPbeta   STAT3	cFos can be activated by any one of p38 [104], JNK [104], Elk1 [103, 105, 106], CEBPbeta [103] or STAT3 [107].
AP1	cJun & cFos	AP1 complex consists of both cJun and cFos [104, 108].
MPK1	AP1	AP1 activates MPK1 [96, 109, 110].
IL8	NFKB   AP1   CEBPbeta	IL8 is activated by anyone of NFKB [31, 111, 112], AP1 [31] or CEBPbeta [3] signals.
NIK	TAK1	NIK is activated by TAK1 [91, 92].
IL-6 signaling		
IL6	(NFKB   ERK1_2   CEBPbeta)	IL6 is activated by anyone of NFKB [32, 33], ERK1_2 [113, 114] or CEBPbeta [3, 115] signals.
IL6R	IL6	IL6 binds to and activates IL6 receptor (IL6R) [88, 116].
GP130	IL6	GP130 is activated by IL6 [117, 118].
PI3K	JAK	PI3K is activated by JAK [119].
JAK	IL6R & SOCS3	Active IL6 receptor (IL6R) activates JAK [117], while JAK is inhibited by SOCS3 [120].
Akt	PI3K	Akt is activated by PI3K [121, 122].
mTOR	Akt	mTOR is activated by Akt [123].
SOCS3	STAT3	SOCS3 is activated by STAT3 [124].
<i>GP130, MEK1_2, and ERK1_2 together depend all on the activation of IL6 to form a cyclic signaling cascade</i>		
MEK1_2	GP130 & IL6	MEK1_2 is activated by GP130 [116, 125] as well as IL6 [116].
ERK1_2	MEK1_2 & IL6	ERK1_2 is activated by MEK1_2 [126] and IL6 [127].
Elk1	ERK1_2	Elk1 is activated by ERK1_2 [128].
CEBPbeta	Elk1	CEBPbeta is activated by Elk1 [103].
STAT3	JAK   (cFos & cJun)   mTOR	STAT3 is activated by JAK [119] or mTOR [129]. Alternatively it can be activated in presence of both cFos and cJun [130].

<https://doi.org/10.1371/journal.pcbi.1005741.t001>

RelA binds with p50 to form a transcriptionally active heterodimer (called NFKB in this model). In its inactive state, it is bound with the inhibitor of kappa B (IkB) and resides in the cytoplasm. Upon NF-κB activation, the inhibitor is phosphorylated by the inhibitor of kappa B kinases (IKK) and degraded which releases the RelA/p50 heterodimer to translocate to the nucleus and regulate the transcription of target genes. To investigate the role of RelA on the expression of IL-8, we set NFKB = 0, simulating the ablation of the transcriptionally active heterodimer (Fig 4). The predictions of the model simulations are consistent with knock-out experiments where the absence of RelA caused a significant reduction in IL-8 production in human fibroblast (IMR-90) [7].

We also simulated the overexpression of IkB by constantly activating IkB (IkB = 1) and could show an effect comparable to the knock-out of RelA (Fig 5). In our model the overexpression of IkB leads to the inhibition of IL-8 and IL-6 expression which is in line with a previously published report, where the overexpression of a non-degradable IkBα completely abolishes IL-8 production, among other soluble factors, in human epithelial and cancer cell lines [34].

Another promising knockout described by our network is inhibitor of nuclear factor kappa-B kinase subunit gamma also known as NEMO, which is able to prevent IL-6 and IL-8 expression after DNA damage activated the DNA damage repair apparatus and cell cycle progression has been stopped *in-silico* (Fig 6). In studies with murine NEMO knockout models it has already been shown that murine embryonic fibroblasts (MEFs) isolated from these mice show reduced NF-κB activity and IL-6 secretion upon stimulation with typical NF-κB activators like IL-1 and TNF [35].

**Start state: DNAD=0 IkB=1 MDM2=1**

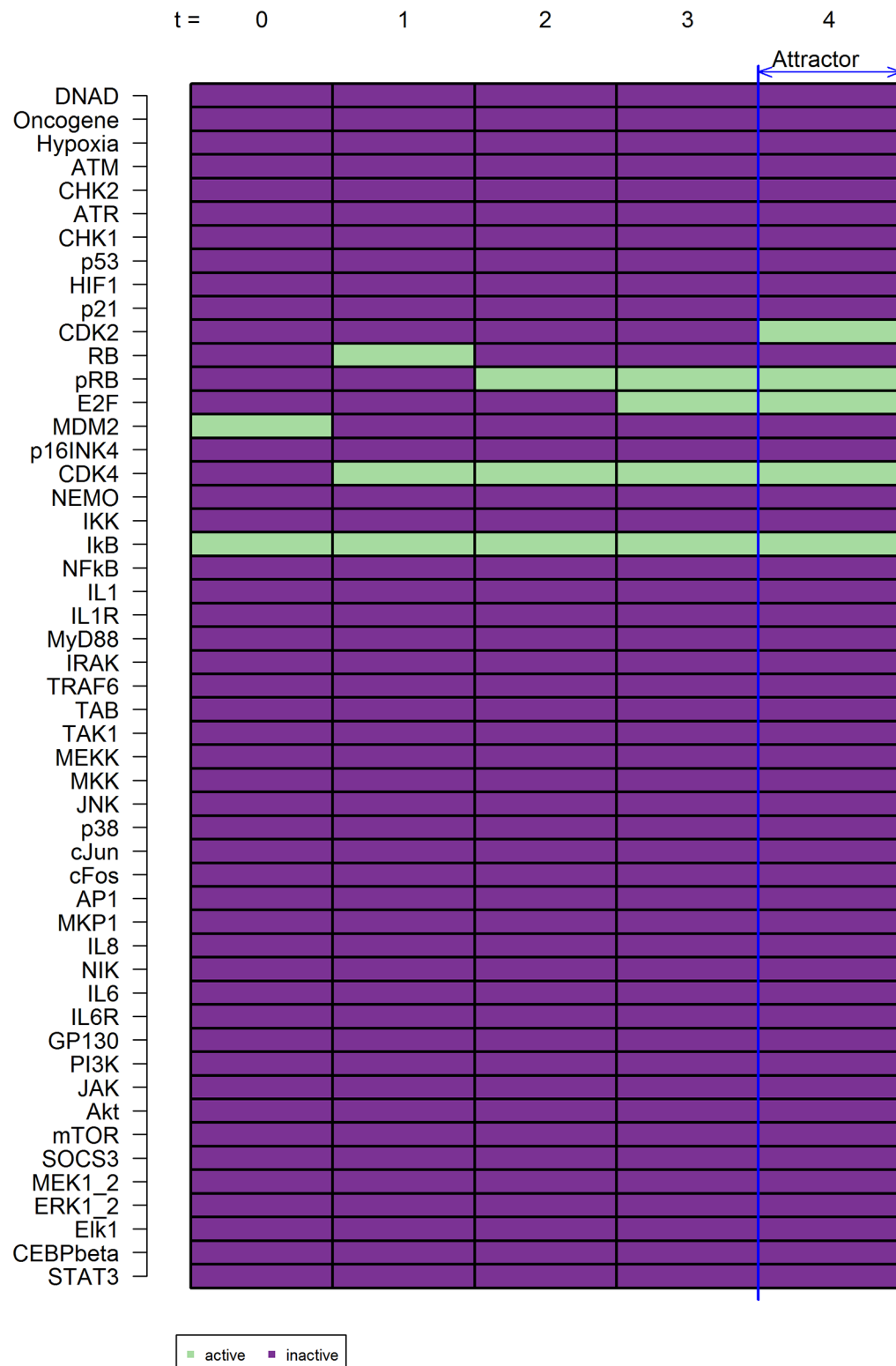


**Fig 2. Naturally occurring network states.** Without DNA damage the resulting network state is expected to show normal cell cycle progression. As shown here this includes the activation of CDK2 ( $t = 5$ ) and CDK4 ( $t = 2$ ) with a subsequent phosphorylation of RB ( $t = 3$ ) leading to a release of E2F ( $t = 4$ ) which will release the cell into cell cycle progression. The temporal sequence is shown as  $t = n$ . Active genes are shown as green, inactive genes as dark purple.

<https://doi.org/10.1371/journal.pcbi.1005741.g002>

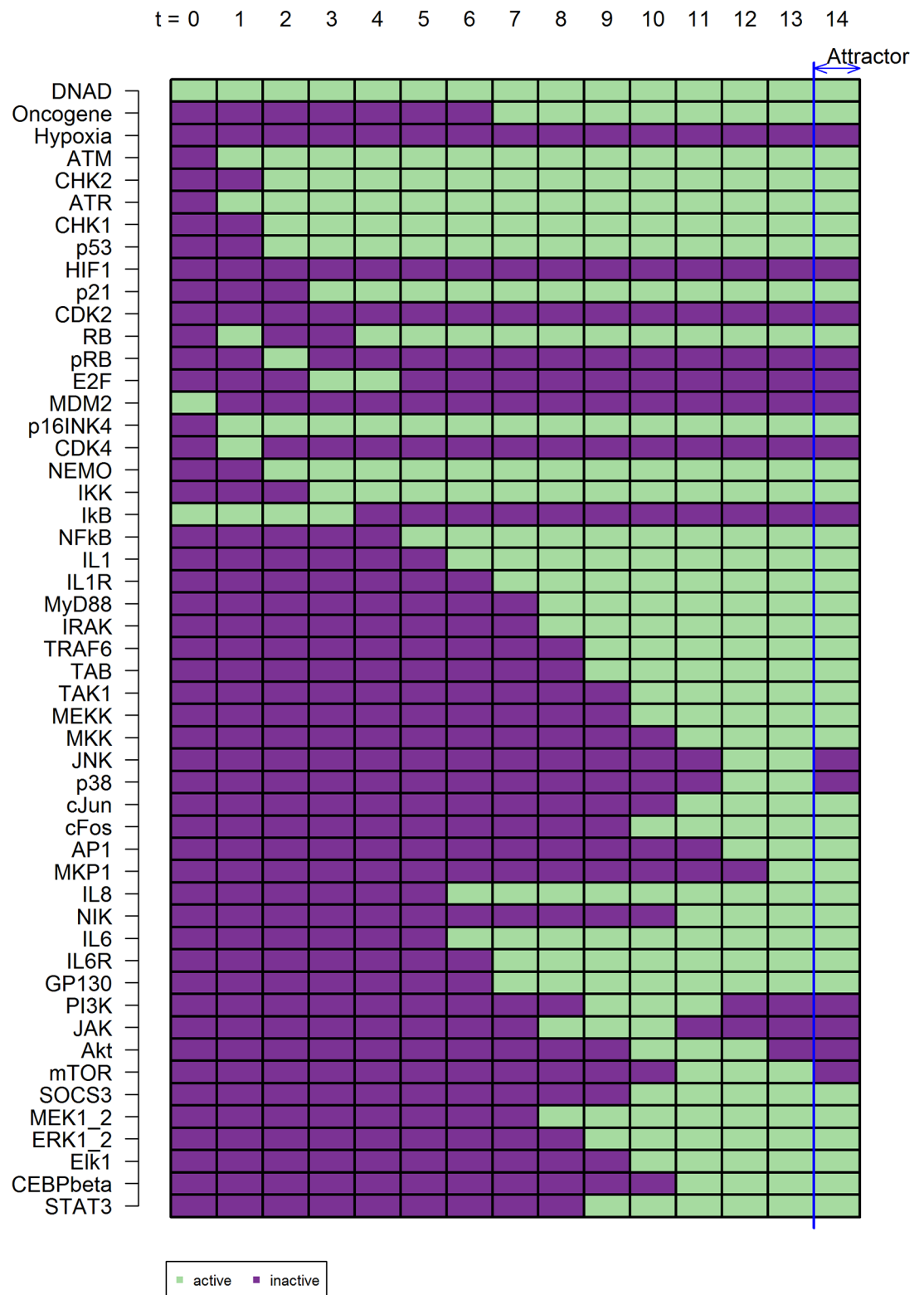
## NEMO is essential for DNA damage triggered NF- $\kappa$ B activation

Apart from being important for the assembly of the IKK-complex, NEMO also acts as a shuttle relaying the ATM-mediated DNA damage apparatus to cellular response mechanisms. Upon DNA damage ATM can bind NEMO and trigger its translocation from the nucleus to the cytoplasm where it activates NF- $\kappa$ B signaling [36]. This in turn will help cells avoid clearance through apoptosis, increasing the number of long-term senescent cells in tissues and organs of the organism and might also increase and sustain the inflammatory potential of the SASP.

In order to evaluate proposed knockouts NEMO was depleted from murine dermal fibroblasts (MDFs) using a NEMO-floxed mouse line. These MDFs were isolated from murine skin and subsequently transfected with a Cre-recombinase coding plasmid including a fluorescence reporter construct (Fig 7). To purify NEMO knockout MDFs, these cells were FACS sorted two days post-transfection (S1A Fig). Successful NEMO knockout was assessed by PCR (S1B Fig) and western blot (S1C Fig). To study the effect of DNA damage, overnight-starved MDFs were treated with 25  $\mu$ M etoposide, an established DNA damage and senescence inducer, for 3 h followed by a 24 h incubation period [37]. Afterwards cell media supernatant was taken and total RNA was isolated. We first measured p21 mRNA expression as an indicator for DNA damage and cell cycle arrest. Without a significant reduction of cell viability (Fig 8A), p21 mRNA expression was upregulated more than twofold in etoposide treated compared to untreated MDFs (Fig 8B). NEMO is of high importance for DNA damage mediated nuclear translocation of the NF- $\kappa$ B signaling molecule p65. As shown by immunofluorescence staining of untreated NEMO wildtype MDFs compared to etoposide treated wildtype and knockout MDFs, the translocation of p65 into the nucleus upon DNA damage is significantly increased in wildtype whereas it is brought down to the level of untreated wildtype MDFs when NEMO is knocked out (Fig 8C).

## NEMO mediates DNA damage induced expression and secretion of IL-6 and IL-8

As we have observed the effect of a NEMO knockout on the nuclear translocation of p65 and thereby activation of NF- $\kappa$ B, we further explored the possible suppressive effect on IL-6 and IL-8 activation. To achieve this we isolated total RNA and analyzed the mRNA expression of IL-6 and the murine homologues of IL-8 CXCL1 (KC), CXCL2 (MIP-2) and CXCL5 (LIX). Upon DNA damage, we observed a significant reduction in IL-6 mRNA expression with a strong downregulation in untreated knockout compared to untreated wildtype. An even stronger downregulation in etoposide treated NEMO knockout compared to wildtype MDFs was detected. Taken together a NEMO knockout could reduce DNA-damage mediated IL-6 mRNA expression by almost tenfold (Fig 9A). Next, we measured the secretion of IL-6. While there is nearly no secretion of IL-6 in untreated wildtype as well as knockout MDFs, a strong increase in IL-6 secretion occurred in etoposide treated wildtype MDFs, whereas the NEMO knockout MDFs only shows a small increase in secretion with a more than hundredfold reduction when compared with etoposide treated wildtype cells (Fig 9B). We additionally analyzed the mRNA expression of three murine IL-8 homologues to assess the impact of a NEMO knockout on DNA damage mediated IL-8 expression. We found that all three chosen

**Start state: DNAD=1 I<sub>k</sub>B=1 MDM2=1**

**Fig 3. Naturally occurring network states upon DNA damage.** Upon DNA damage the first response of the cell is the activation of ATM/ATR mediated DNA damage repair ( $t = 2$ ) with a subsequent activation of p53- and p16-mediated cell cycle arrest ( $t = 3$ ). The DNA damage signal is relayed by the DNA damage response through NEMO ( $t = 3$ ) that in turn activates NF- $\kappa$ B signaling ( $t = 4$ ) which will ultimately lead to the activation of IL-1, IL-6 and IL-8 signaling ( $t = 7$ ). The temporal sequence is shown as  $t = n$ . Active genes are shown as green, inactive genes as dark purple.

<https://doi.org/10.1371/journal.pcbi.1005741.g003>

homologues were significantly downregulated in NEMO knockout MDFs compared to wild-type MDFs after DNA damage. The total expression of IL-8 homologues mRNA in NEMO knockout MDFs was reduced by at least fivefold when compared to treated wildtype MDFs (Fig 9C). There is detectable secretion of IL-8 homologues in untreated wildtype and NEMO knockout MDFs, however the secretion strongly rose upon etoposide treated in wildtype cells whereas there is no detectable increase in the NEMO knockout MDFs. This effect was similarly found for the studied IL-8 homologues KC and MIP-2 (Fig 9D). However, we did not find any significant alteration in the expression of two housekeeping genes, such as beta-actin and 18s rRNA in the NEMO knockout MDFs, compared with NEMO wildtype (S2A Fig). In addition, we also did not observe any significant alteration in the expression of a wide array of genes that were predicted by Boolean network not to be changed after NEMO knockout (S2B Fig). These data show the importance of NEMO and NF- $\kappa$ B signaling for the activation of IL-6 and IL-8 in the case of DNA damage. In early stages DNA damaged and cell cycle arrested MDFs most likely activate secretory SASP signaling through NF- $\kappa$ B rather than other stress pathways.

## Discussion

In the model of DNA damage and proinflammatory signaling presented here we collected and combined previously published knowledge on major regulators of the SASP. Using this model, we identified attractors fitting cell cycle progression and cell cycle arrest as they physiologically occur. This suggests reliability of this model in terms of reproducibility of current biological knowledge. The network model allows us to time- and cost-effectively generate hypotheses and predict gene knockouts that may influence the outcome of the SASP *in-vitro*.

In the process of modeling, we first created individual models of DNA damage and proinflammatory signaling. In a next step, we fused these two sub-networks to the model presented here. In S1 Text, we analyzed the impact of integrating both pathways in one Boolean network model. Our results indicate that there is not only an effect of DNA damage in the proinflammatory signaling but also vice versa. On one hand, we deduce a stabilization of the DNA damage response network as the integration of both sub-networks leads to a reduction of possible attractors (87 to 19). On the other hand, the inner dynamics of each sub-network stay intact, showing biologically reproducible signaling cascades (e.g. Fig 4).

In the simulation without DNA damage, only activation of cell cycle regulation genes that facilitate cell cycle progression were observed [38]. In contrast, when we entered DNA damage into the network, we detected early activation of the DNA damage response (DDR) followed by a p53/p21 mediated cell cycle arrest and at a later time point the activation of proinflammatory signaling through NF- $\kappa$ B [39, 40]. We utilized the Boolean network to simulate knockout and overexpression states that have the power to inhibit both IL-6 and IL-8 activation, such as knockouts of ATM and RelA or the overexpression of I $\kappa$ B $\alpha$ , that have previously been published to decrease IL-8 or IL-6 expression and secretion *in-vitro* [7, 9, 34]. One of the most prominent knockout suggestions obtained was that of NEMO, which acts as an essential modulator of NF- $\kappa$ B signaling and is a major link between DDR and NF- $\kappa$ B signaling [41]. Therefore, it is a suitable target to prevent NF- $\kappa$ B activation, while maintaining the repair potential of the DDR. Taken together these *in-silico* data suggest NF- $\kappa$ B to be one of the major SASP

**Start state: DNAD=1 I<sub>k</sub>B=1 MDM2=1  
NF<sub>k</sub>B knockout**

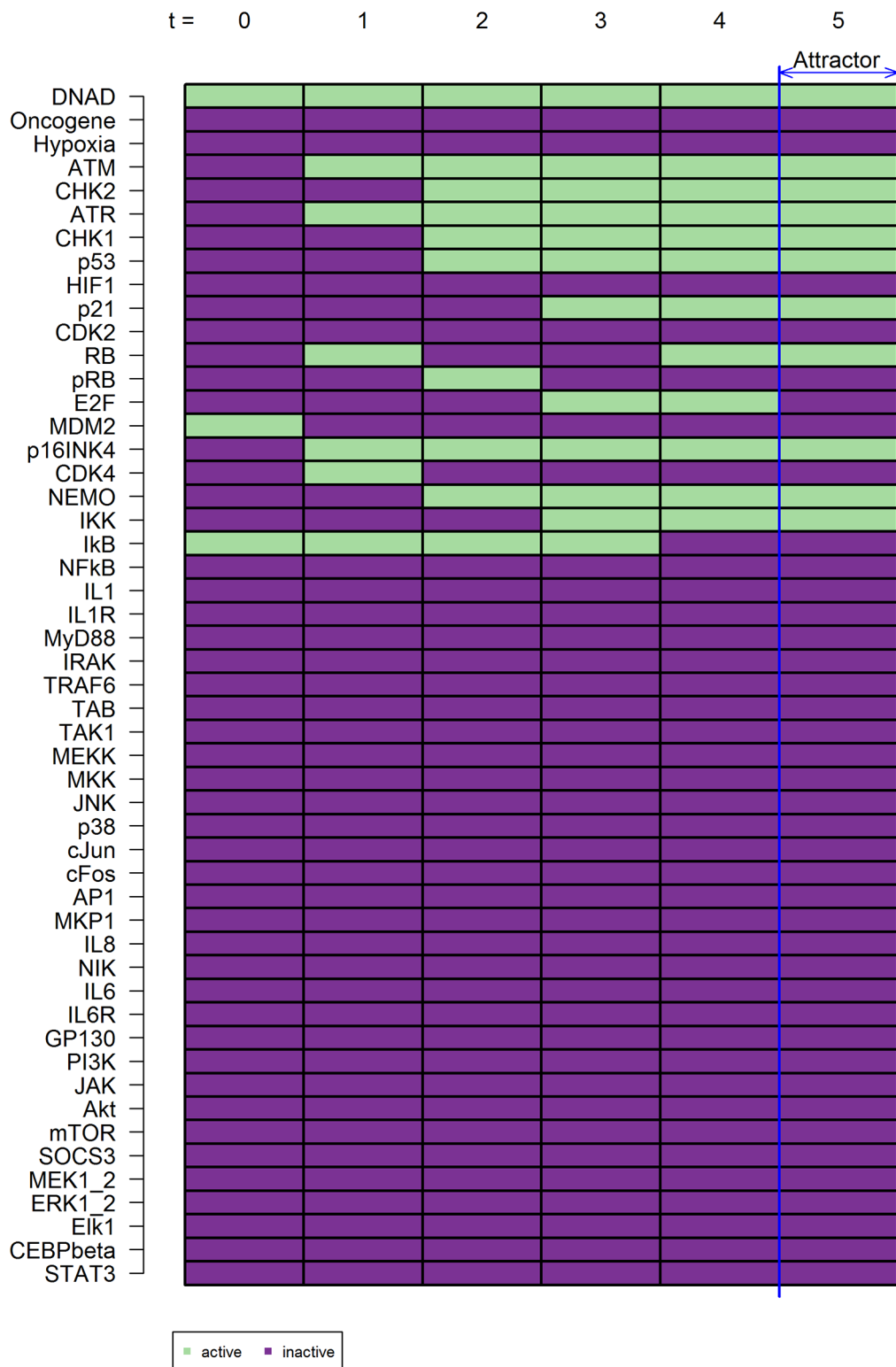


**Fig 4. Knockouts that cause *in-silico* IL-6 and IL-8 inhibition for NFκB knockout.** Network states present the gene activity of all genes in the model. Green boxes indicate gene activation while red boxes show gene inactivation. A knock-down or overexpression is simulated by setting a gene to 0 or 1, respectively. This simulation shows the time course of expected states after DNA damage with NF-κB switched off ( $NF\kappa B = 0$ ) which leads to an inhibition of proinflammatory signaling.

<https://doi.org/10.1371/journal.pcbi.1005741.g004>

activators in response to DNA damage activating all three mediators of proinflammatory signaling depicted in this network.

For the sake of manageability, the model presented here was limited to a core set of pathways involved in senescence and the SASP. Of course, the value of the results could still be enriched by adding even more components and additional pathways, such as a more detail view on CEBP-signaling, growth factor signaling and the expansion of cell cycle related signaling. This would enable to simulate an even deeper level of signaling involved in the SASP.

Another factor that was not viewed in this work is the influence of the intensity levels and timing of expression and stimuli on the outcome of the SASP. Physiologically occurring DNA damage, for example, is not an all or nothing event but rather comes in different levels and lengths of damage that can trigger a multitude of different reactions in the cell. In future works, it would be interesting to add these into the model. Such extension would allow simulations of the exact amount and timing of damage needed to trigger full-blown SASP rather than senescence. Furthermore, it would possibly reveal at which point the cell decides that it is beneficial to trigger SASP signaling in order to warn the system of the damage and initiate clearance as opposed to trying to repair itself.

IL-6 and IL-8 reinforce senescence in an autocrine and paracrine way, concomitantly preventing senescent cells from exiting cell cycle arrest and forcing neighboring cells into senescence themselves [3, 42]. Persistent DDR activity, that is also known to induce IL-6 and IL-8 secretion [9], could be shown in various premalignant and malignant lesions *in-vivo*, and is hypothesized to be one the main causes of aging [9, 43, 44]. Due to this ability to promote invasiveness of cancer cells and the spreading of senescence to neighboring cells IL-6 and IL-8 are of special interest [3, 45]. While it is probably not detrimental to transiently activate the respective signaling pathways, the long-term persistence of unrepairable DNA damage leads to a lasting activation of NF-κB through the DDR mechanisms and thereby to a prolonged stimulation of IL-6 and IL-8. Ultimately, this initiates and perpetuates a vicious cycle from which cells cannot escape and causes the development of the SASP.

To explore and validate previously generated *in-silico* results *in-vitro*, we isolated murine dermal fibroblasts from NEMO-floxed mice and transfected these with a Cre-recombinase plasmid to deplete NEMO. Contrary to NEMO knockout MDFs we observed RelA enrichment in the nucleus in DNA damaged wildtype cells. This suggests that mainly NEMO is responsible for the forwarding of DNA damage signals from the DDR to NF-κB signaling.

We were particularly interested in achieving inhibition of IL-6 and IL-8 expression and secretion *in-silico* and *in-vitro*. As we could show in our *in-vitro* results, DNA damaged NEMO knockout cells did not reveal any induction of IL-6 or IL-8 homologue mRNA expression, suggesting that DNA damage-triggered IL-6 and IL-8 expression is mainly conferred by NF-κB signaling. This was confirmed on protein level, showing a strong decrease in secretion of both IL-6 and IL-8 homologues in NEMO knockout MDFs. In conclusion, abolishing NEMO is sufficient to not only block the signaling from DDR to NF-κB but also to decrease expression and secretion of two of the most prominent and established SASP mediators IL-6 and IL-8.

The question arises why damaged senescent cells have to start expressing and secreting factors that are detrimental to themselves, surrounding cells and tissues. The secretion of many SASP factors can be explained firstly by the attempt to clear senescent cells from tissue by cells

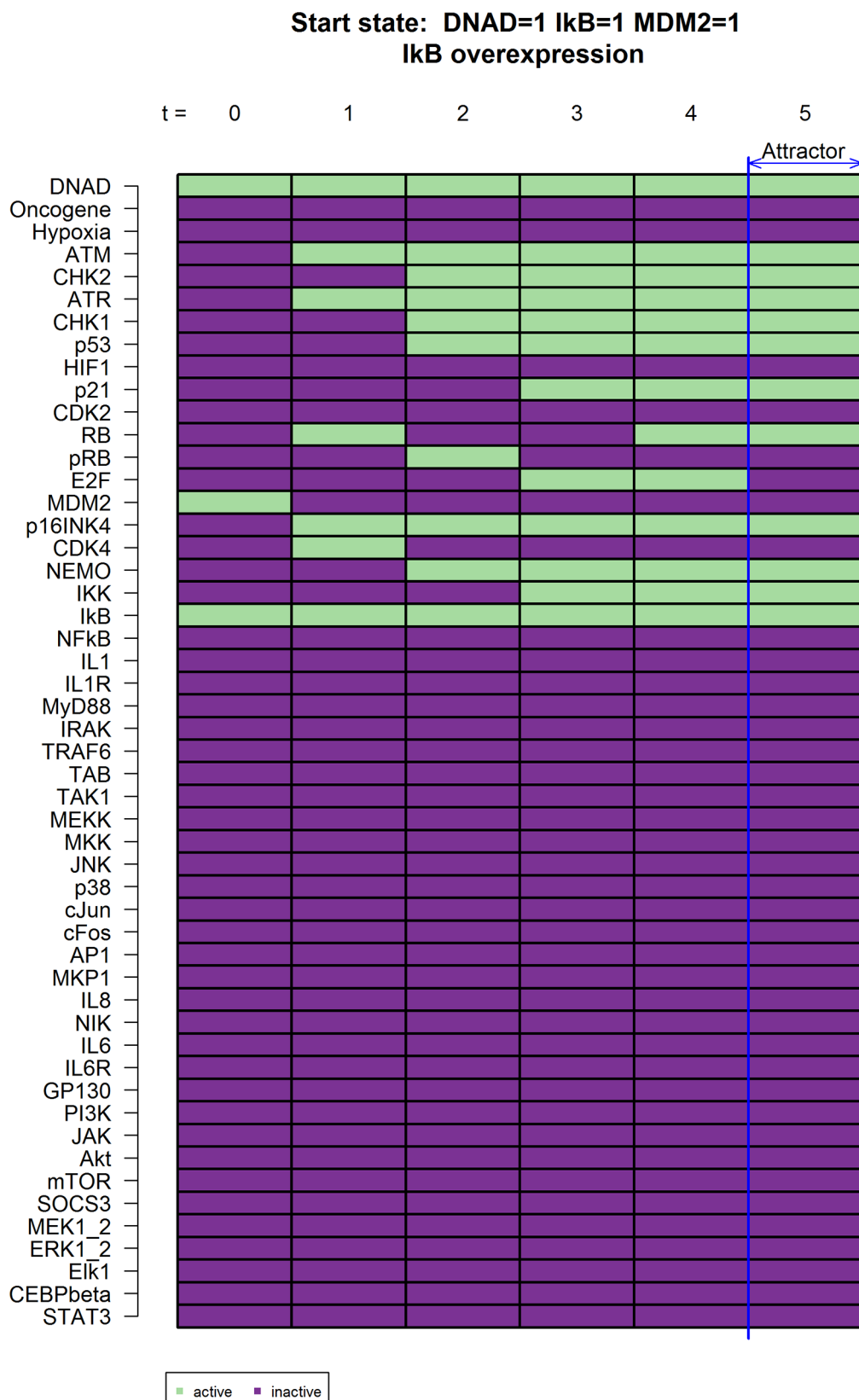


**Fig 5. Knockouts that cause *in-silico* IL-6 and IL-8 inhibition for I<sub>k</sub>B overexpression.** This simulation shows an overexpression of I<sub>k</sub>B (I<sub>k</sub>B = 1) showing a similar outcome as in Fig 4.

<https://doi.org/10.1371/journal.pcbi.1005741.g005>

**Start state: DNAD=1 I kB=1 MDM2=1  
NEMO knockout**

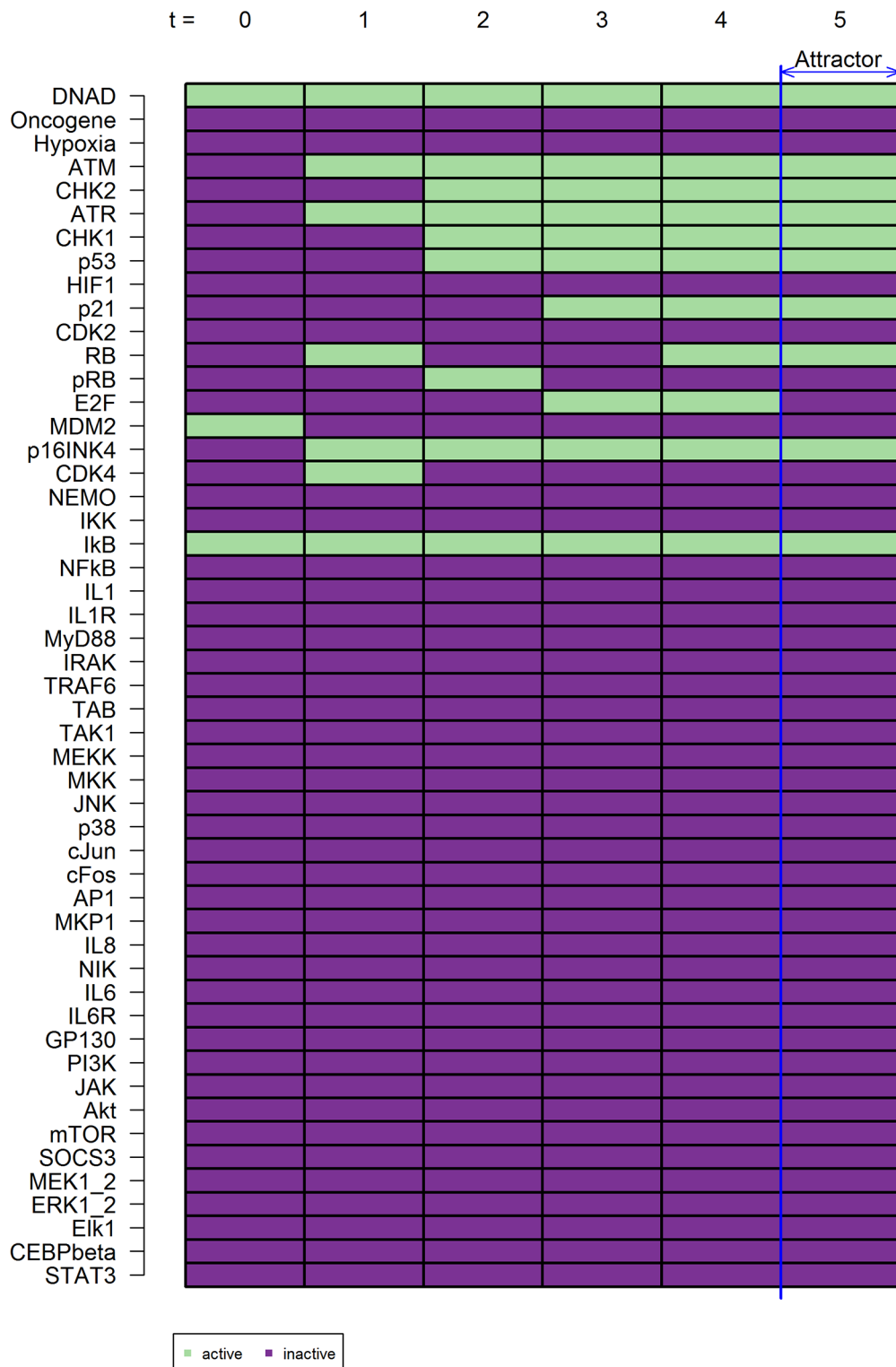


**Fig 6. Knockouts that cause *in-silico* IL-6 and IL-8 inhibition for NEMO knockout.** NEMO is switched off (NEMO = 0) preventing NF- $\kappa$ B signaling from being activated. The outcome is similar to the two previously described simulations in Figs 4 and 5.

<https://doi.org/10.1371/journal.pcbi.1005741.g006>

of the innate immune system and secondly as a warning to the microenvironment that there is a danger in the near vicinity. Senescent cells secrete different factors that attract phagocytic immune cells and induce proteolytic enzymes to facilitate their migration through the extracellular matrix [46]. As long as damaged cells can be cleared in early phases the SASP is probably beneficial for the organism, however once the immune system cannot keep up with the emergence of damaged cells, detrimental effects accumulate and tissue takes damage [2, 47]. In this phase, it would be beneficial to have the possibility to counteract the SASP and give the immune system time to catch up.

In summary, we could illustrate that *in-silico* identification of genes with mechanistic contribution in the regulation of the SASP, confirmed under experimental conditions *in-vitro*, is a highly suitable approach and holds substantial promise to identifying therapeutic targets to delay or even prevent the detrimental SASP effects on tissue homeostasis and overall ageing. Using our Boolean model, we were able to reproduce published data *in-silico* and generate various knockout proposals to shut down two of the most detrimental effectors of the SASP. This is of major clinical relevance in terms of tissue aging. In fact, SASP factors like IL-6 and IL-8 have been correlated with inflamming not only driving the aging process itself, but also

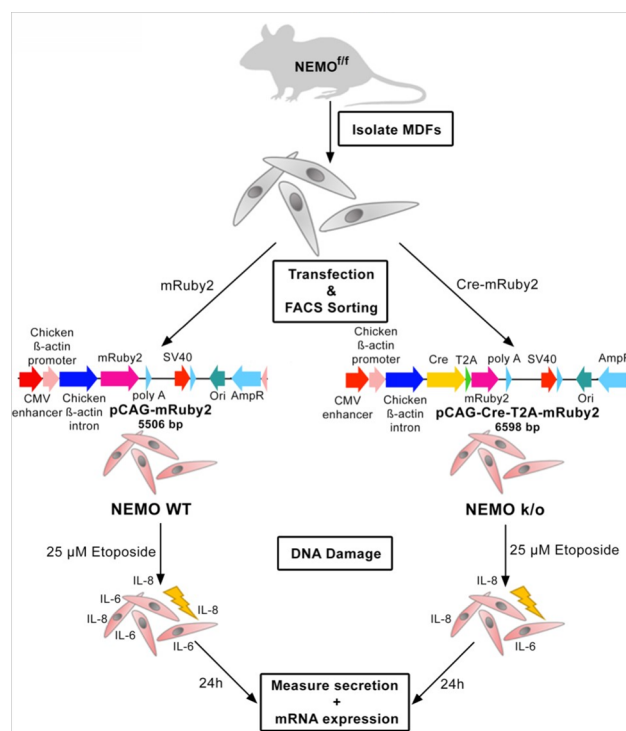


**Fig 7. Schematic overview of the experimental workflow.** Murine dermal fibroblasts (MDFs) are isolated from NEMO-floxed mice. After short expansion in cell culture these MDFs are transfected with pCAG-Cre-T2A-mRuby2 or pCAG-mRuby2, respectively. Because of mRuby2 expression, successfully transfected cells can be sorted by FACS. Cells transfected with pCAG-Cre-T2A-mRuby2 are knocked out for NEMO while pCAG-mRuby2 transfected cells are used as wildtype controls. After transfection cells are treated with 25  $\mu$ M etoposide for 3 h to induce DNA damage. 24 h after treatment cell culture media is taken for ELISA measurement of secretion and cells are harvested for RNA isolation and subsequent RT-qPCR analysis.

<https://doi.org/10.1371/journal.pcbi.1005741.g007>

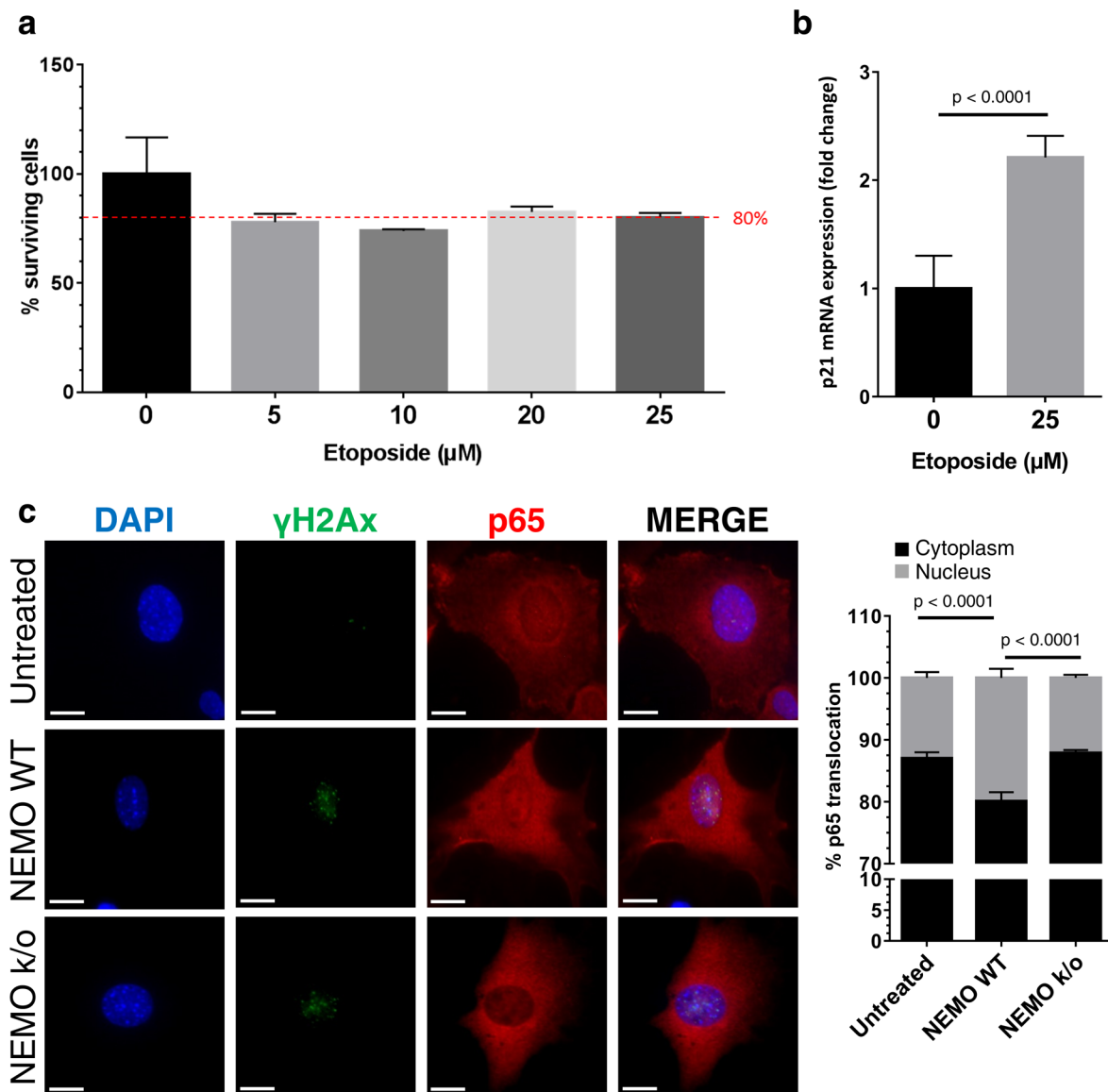


**Fig 8. NEMO knockout murine dermal fibroblasts show a decreased nuclear translocation of p65.** **a.** MTT assay determined optimal experimental conditions. 80% viable cells was set as threshold. After overnight serum starvation MDFs were treated with etoposide for 3 h followed by a 24 h incubation period. MTT assay was started afterwards to determine the viability of cells. Values are presented as mean  $\pm$  SEM in percent. ( $n = 3$ ) **b.** In order to evaluate DNA damage response and cell cycle arrest mRNA expression of p21 was analysed by RT-qPCR in MDFs treated with 25 $\mu\text{M}$  etoposide for 3 h followed by a 24 h incubation time ( $n = 5$ ). Values are presented as mean  $\pm$  SEM of fold change. Comparison was made with two-tailed t-test;  $P$ -value indicated the significance of difference. **c.** Representative immunostaining of  $\gamma\text{H2Ax}$  (green) and p65 (red) in wildtype (NEMO WT) and NEMO knockout (NEMO k/o) MDFs treated with 25 $\mu\text{M}$  etoposide for 3 h with a following incubation period of 24 h. Scale bars, 50 $\mu\text{m}$ . The graph shows the percentage of p65 in the cytoplasm (black bars) compared to the nucleus (grey bars) as percentage of red pixels. Values are mean  $\pm$  SEM in percent. Comparison was made with two-tailed t-test ( $n = 10$ ); line and  $P$ -value.

<https://doi.org/10.1371/journal.pcbi.1005741.g008>

promoting aging associated morbidity, frailty and mortality [48]. We additionally were able to validate and prove one of the most prominent knockout suggestions *in-vitro*, keeping in mind that there might always be detrimental off-target effects when altering a major signaling pathway like NF- $\kappa$ B. However, targeting NEMO and its interaction partners, as already shown in

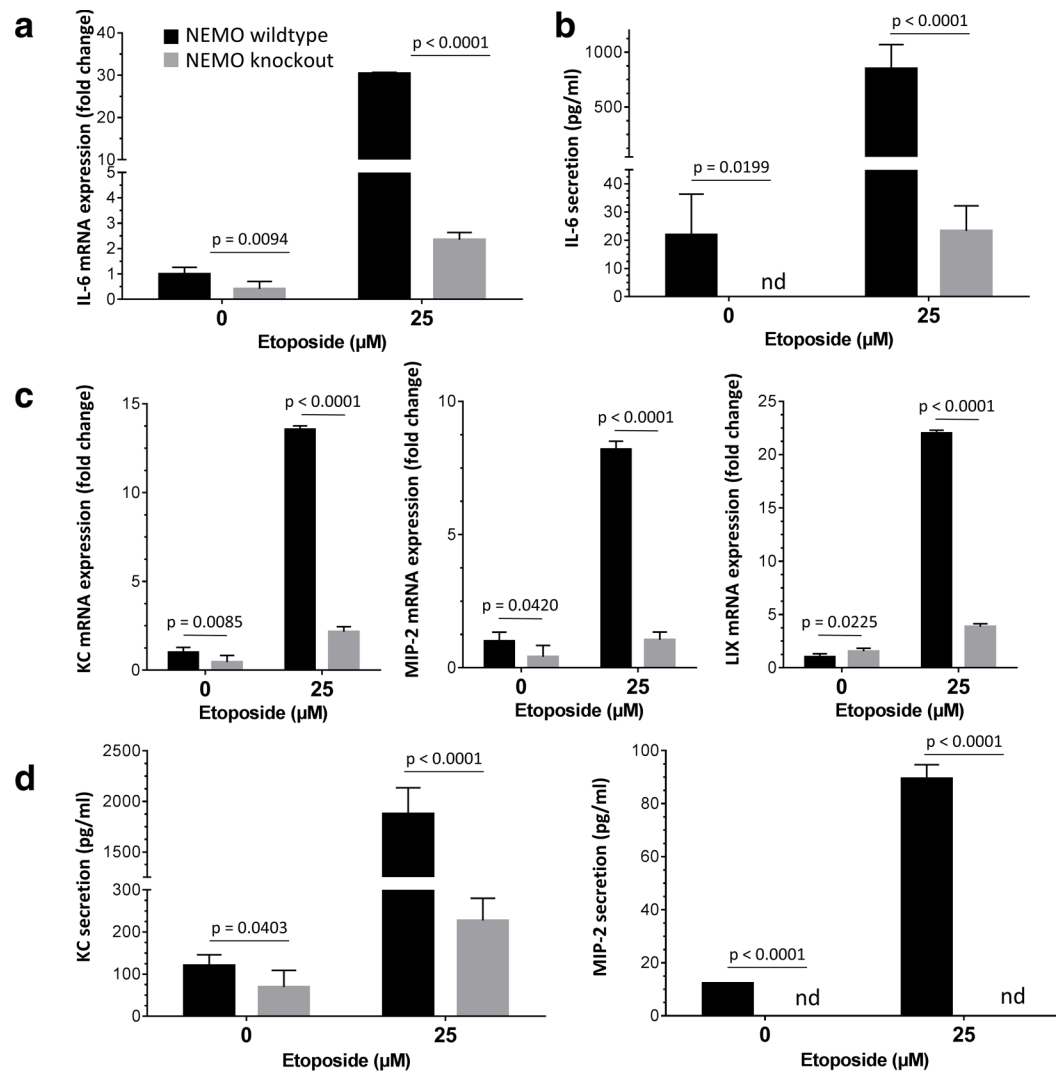


**Fig 9. DNA damaged NEMO knockout MDFs show a decrease in IL-6 and IL-8 mRNA expression and protein secretion.** **a.** To assess the influence of the NEMO knockout on DNA damage mediated activation of SASP signaling IL-6 mRNA expression was measured by RT-qPCR in untreated and etoposide-treated MDFs ( $n = 5$ ). Cells with wildtype NEMO (black bars) or NEMO knockout (grey bars) were used. Values were presented as mean  $\pm$  SEM of fold change. Comparison was made with the two-tailed t-test. **b.** IL-6 secretion was measured by ELISA in conditioned media of untreated and etoposide-treated MDFs ( $n = 5$ ). Cells with wildtype NEMO (black bars) or NEMO knockout (grey bars) were used. Values were presented as mean  $\pm$  SEM of total secretion in pg/ml, nd means non-detectable. Comparison was made with the two-tailed t-test. **c.** In addition to IL-6 murine IL-8 homologues KC, LIX and MIP-2 were used to further show activation of SASP signaling. mRNA of all three homologues was measured by RT-qPCR in untreated and etoposide-treated MDFs ( $n = 5$ ). Cells with wildtype NEMO (black bars) or NEMO knockout (grey bars) were used. Values were presented as mean  $\pm$  SEM of fold change. Comparison was made with the two-tailed t-test. **d.** IL-8 homologue secretion was measured by ELISA in conditioned media as previously described ( $n = 5$ ). Values were presented as mean  $\pm$  SEM of total secretion in pg/ml, nd means non-detectable. Comparison was made with the two-tailed t-test.

<https://doi.org/10.1371/journal.pcbi.1005741.g009>

studies of inflammatory arthritis and diffuse large B-cell lymphoma, may hold promise for the development of new therapies for age-related pathologies in which senescence and the SASP play a role [49, 50].

## Methods

### Mice experiments

Murine dermal fibroblasts from an inducible connective tissue-specific NEMO-deficient mouse model were used for *in-vitro* experiments. This mouse line (Col(I) $\alpha$ 2-CreERT $^+$ ; NEMO $^{ff}$ ) was generated by crossing Col(I) $\alpha$ 2-CreERT transgenic mice [51] with NEMO floxed mice [35]. These mice were backcrossed to C57BL/6J for at least 6 generations. They were maintained in the Animal Facility of the University of Ulm with 12 h light–dark cycle and SPF conditions. The breeding of the mice and all experiments were approved by the animal ethical committee (approval number, Tierversuch-Nr. 1102, Regierungspräsidium Tübingen, Germany). For mice genotyping standard PCR techniques were used. The sequences of the primers used in this manuscript are summarized in S1 Table. Briefly, DNA was isolated from the tail tip of an individual mouse using a commercial kit (Easy DNA kit, Invitrogen). Purified DNA was later dissolved in TE and used for PCR amplification. The PCR products were run in QIAxcel Advance system (Qiagen) using the program AM320 and then documented digitally.

### Isolation and culture of murine dermal fibroblasts

Murine dermal fibroblasts (MDFs) were isolated from ear skin of young mice and cultured as previously described [52].

### Induction of DNA damage

DNA damage was induced by adding etoposide to cell culture media at a concentration of 25  $\mu$ M for 3 hours after overnight serum-starvation. Supernatants subsequently removed and cells were rinsed with PBS before adding fresh culture media. Cells and/or media were used 24 h later for further analysis.

### Cloning

Recombineering technology [53] was used to construct plasmids containing CDS of both Cre recombinase and fluorescence reporter, mRuby2 or only mRuby2. pCAG-Cre vector (a gift from Connie Cepko, Addgene plasmid # 13775) was used for the recombineering. In the first construct, the aim was to insert the T2A-mRuby2 sequence before the stop codon of Cre recombinase and in the second construct, the aim was to replace the Cre ORF with mRuby2 ORF. In brief, synthetic DNA fragments were synthesized either as gBlock (IDT) or as GeneArt string (Thermo Scientific). Four DNA fragments were synthesized, the first one contained 5' 50 bp homology regions to the vector (targeting 50 nucleotide upstream of Cre ORF stop codon), chloramphenicol and ccdB cassettes and 3' terminal 50 bp homology regions to the vector (targeting 50 nucleotide downstream of last amino acid coding codon of Cre ORF, i.e., codon preceding the Cre ORF stop codon). The second synthetic fragment contained 5' 50 bp homology regions to the vector (targeting 50 nucleotide upstream of Cre ORF start codon), chloramphenicol and ccdB cassettes and 3' terminal 50 bp homology regions to the vector (targeting 50 nucleotide downstream of Cre ORF stop codon). The third synthetic fragment contained 5' 50 bp homology regions to the vector (same as fragment 1), T2A sequence-mRuby2 ORF and 3' terminal 50 bp homology regions to the vector (same as fragment 1). The fourth synthetic fragment contained 5' 50 bp homology regions to the vector (same as fragment 2), mRuby2 ORF and 3' terminal 50 bp homology regions to the vector (same as fragment 2). E. coli containing pCAG-Cre was processed for electrocompetent using standard methods and these electrocompetent E. coli, containing pCAG-Cre were electroporated with a dual inducible

expression plasmid pSC101-ccdB-gbaA (a gift from Prof. A. Francis Stewart) and selected for ampicillin 100 $\mu$ g/ml and tetracycline 3.5 $\mu$ g/ml at 30°C. Next day, 4–5 colonies were expanded and the expression of recombineering proteins,  $\lambda$ phage *red $\alpha$* , *red $\beta$*  and *red $\gamma$*  and *recA* (*redgbA*) was induced by L-rhamnose (1.4mg/ml). After 1 h of L-rhamnose treatment, the induced E. coli were processed for electrocompetent and then electroporated either with synthetic DNA fragments 1 or 2. After 1 h of recovery in SOC medium, the electroporated E. coli, were plated in LB-agar containing ampicillin 100 $\mu$ g/ml, tetracycline 3.5 $\mu$ g/ml, chloramphenicol 25 $\mu$ g/ml and 1.4mg/ml L-arabinose. L-arabinose addition induced the expression of ccdA, the antidote of ccdB in that only recombined plasmid containing E. coli can survive. Thereafter colonies from fragment 1 and fragment 2 electroporated E. coli plates were picked and expanded for the verification of first recombinant product using restriction digestion analyses. The corresponding colony was expanded and *redgbA* expression was induced by L-rhamnose for 1 h. The induced E. coli containing either recombined DNA fragment 1 or fragment 2 were made electrocompetent for the second round of recombineering. The E. coli, containing recombined DNA fragment 1 then electroporated with synthetic DNA fragment 3. The E. coli, containing recombined DNA fragment 2 were electroporated with synthetic DNA fragment 4. The recovered electroporated E. coli were plated in LB-agar containing ampicillin 100 $\mu$ g/ml and incubated at 37°C overnight. Colonies from both plates were picked, expanded and verified for the second recombinant products. The correct plasmids were sequenced and verified through commercial services (Sequiserve, Germany). Plasmid preparation was performed using a commercially available kit (Qiagen plasmid plus kit, Qiagen). This plasmid (pCAG-Cre-T2A-mRuby2) can be obtained from the authors on request and was deposited in the Addgene repository (Accession ID 102989).

### Initiation of Cre activity (NEMO knockout)

Early passage MDFs with a floxed NEMO allele were transfected with a Cre expressing vector using an electroporation-based transfection method (Amaxa, Lonza Group). Transfer of the plasmid was performed using a commercial kit with the AMAXA program N24 (Nucleofector Kits for Mouse or Rat Hepatocytes, Lonza). Successful NEMO knockout was assessed by PCR as explained before.

### FACS sorting of positive cells

Two days after transfection cell populations were purified using the mRuby2-based reporter system included in the previously described Cre-expressing vectors. Gating was set for living cells and singlets, sorting was based on mRuby2 expression in the PE-channel. FACS-sorting was performed with a FACSaria III system (BD Biosciences) and analysis was done on FACS-Diva and FlowJo (Tree Star) software.

### Immunofluorescence staining

Cells were fixed in 4% PFA in PBS for 15 min and thereafter treated with 0.1% Triton X-100 for 10 min at room temperature. Blocking was performed in 5% BSA for 1 h at room temperature. Anti-p65 (#8242, 1:200, Cell Signaling) and anti- $\gamma$ H2A.x (ab22551, 1:200, Abcam) were used as primary antibodies overnight at 4°C. Incubation with the secondary antibody Alexa 488 goat anti-mouse (for  $\gamma$ H2A.x, 1:500) and Alexa 555 goat anti-rabbit (for p65, 1:500) was performed at room temperature for 1 h.

## Western blotting

Western blot analyses were performed as described earlier [54]. In brief, murine dermal fibroblasts were lysed in RIPA lysis buffer (25mM Tris-HCl pH 7.6, 150mM NaCl, 1% NP-40, 1% sodium deoxycholate, 0.1% SDS) supplemented with protease and phosphatase inhibitors (Thermo Scientific). Cells in RIPA were sonicated using sonopuls HD 2070 and MS72 microtips (Bandelin). The sonicator setting was 50% power 3 cycles and 10 sec for three times. Following sonication, the lysate was centrifuged for 15 min at 14000 rpm and 4°C. The supernatant was collected and protein concentration was measured by Bradford Assay (Biorad). 50µg of protein from each lysate was resolved in 4–20% SDS-PAGE, followed by transfer to nitrocellulose membrane and probing the membrane with anti-NEMO antibody (1:1000, Abcam). The membrane was incubated with goat anti-rabbit IgG coupled with HRP for 1 hr (Jackson ImmunoResearch). Thereafter the membrane was developed by LumiGLO chemiluminescence reagent (Cell Signaling Technologies) using Fusion FX7 Gel-doc system (Vilber Lourmat), followed by stripping with Restore Plus Western blot Stripping Buffer (Thermo Scientific) and re-probed with anti-β-actin antibody coupled with HRP (1:12000, Santa Cruz), finally developed the membrane using LumiGLO.

## Quantitative PCR

Twenty-four hours after treatment, total RNA was isolated from cultured murine dermal fibroblasts using a commercial kit (RNeasy Mini Kit, Qiagen) as described by the manufacturer. Two µg of RNA per sample were reverse transcribed using illustra Ready-To-Go RT-PCR Beads (GE Healthcare). Quantity and quality of total RNA and cDNA was assessed using Nanodrop 1000 (Thermo Scientific) and QIAxcel Advance system (Qiagen). The 7300 real time PCR system (Applied Biosystem, Life Technologies) was used to amplify cDNA using Power SYBR green mastermix (Applied Biosystems, Life Technologies). Sequences for primers used in all experiments and genotyping are provided in [S1 Table](#).

## ELISA

After etoposide treatment cells were supplied with fresh culture media. Culture media was taken for analysis of secreted IL-6 and murine IL-8 homologues (KC and MIP-2) 24 h after treatment. Media was stored at -80°C until analysis.

Concentrations of secreted IL-6 and murine IL-8 homologues after DNA damage were determined using commercial kits (Mouse IL-6/KC/MIP-2 Quantikine ELISA Kit, R&D) as described by the manufacturer.

## Statistical calculations

The influence of a NEMO knockout was compared to wildtype controls based on IL-6, IL-8 homologue and p21 mRNA expression as well as IL-6 and IL-8 homologue protein secretion. The sample size for all experiments was 5 per group. The expression and secretion of the two groups was tested using unpaired two-tailed t-test. Furthermore, the influence of the NEMO knockout compared to wildtype controls on the nuclear translocation of p65 was measured by the percentage of fluorescence intensity in the cell nucleus as well as cytoplasm (sample size = 10). The fluorescence intensity was tested using unpaired two-tailed t-test. The exact p-values are depicted in the respective figures. The figures show mean values. Error bars correspond to the standard error of the mean.

## Boolean networks

In a first step, IL- and DNA-damage pathways included in the Boolean model of SASP were reconstructed individually. To generate the independent gene regulatory networks of inflammatory and DDR signaling, we collected peer-reviewed literature that is considered relevant in the context of SASP (see [Table 1](#)). This literature reports data about the local interaction of key genes regulating each pathway. The information was collected in murine and human experimental *in-vivo* and *in-vitro* studies. In order to control the complexity of model we restricted the set of regulatory factors in the model to the most relevant for SASP and to those being important components of each pathway. The modeled pathways were chosen based on the requirement in the onset and maintenance of the SASP shown in studies related to senescence and the SASP. In total 80 publications were used to determine the relationships between the individual components of the model ([Table 1](#)).

After the reconstruction of Boolean network models of inflammation and DNA damage response, both were combined into a larger network. The impact of combining the two network models instead of simulating them independently is shown by additional analysis in [S1 Text](#). Simulations based on specific environmental (input) conditions were performed to find the corresponding attractors. Furthermore, to identify possible interaction targets, i.e., to generate testable hypotheses about interventions, we fixed corresponding regulatory factors to either 0 or 1 (modelling of knockout or overexpression, similar to [55]) and reran the simulations ([S1 Text](#)). Given an interaction target, we looked for the attractors that positively influence the DNA damage response phenotype.

Network figures were drawn with Biotapestry ([www.biotapecstry.org](http://www.biotapecstry.org)). Simulations of the Boolean network were performed with the package BoolNet [12, 56] in R ([www.r-project.org](http://www.r-project.org)).

This model contains two external signals (DNA damage and Activated Oncogenes). These signals do not coincide with genes within the network, but represent different stimuli from external or internal sources that are known to activate the DNA damage response and/or cell cycle arrest signaling through either p16<sup>INK4</sup> or p53/p21.

## Supporting information

**S1 Fig. Establishment of a pure NEMO knockout murine dermal fibroblast (MDF) population.** **a.** To purify NEMO k/o MDFs, NEMO-floxed cells were transfected with a Cre-recombinase vector including a mRUBY2-reporter construct. Two days post-transfection cells were purified for the NEMO k/o using flowcytometry-based sorting, gating for living cells, cell singlets and mRUBY2 signal (histograms; left to right). **b.** Successful NEMO k/o was determined using PCR analysis. DNA was isolated from FACS-sorted MDFs and later used for PCR amplification. Cre-recombinase activity induced the deletion of floxed NEMO alleles resulting in a bigger sized amplification product in successful knockouts as compared to wildtype cells. **c.** In addition to PCR analysis a successful knockout on protein level was determined by western blotting of cell lysates equilibrated to actin expression levels.  
(TIF)

**S2 Fig. Unaltered expression of selected genes (predicted to be unaffected in NEMO knockout) following NEMO knockout.** The expression level of a set of genes that were predicted not to be changed after NEMO knockout by the Boolean network model. In a setting of 2-fold cutoff (blue dotted line), the expression of all genes remained unaltered between control and NEMO knock out MDFs. Dotted line at value '1' represents level of expression in the control MDFs.  
(TIF)

**S1 Table. Primer sequences.**  
(DOCX)

**S1 Text. Simulation of SASP network with BoolNet.**  
(PDF)

## Author Contributions

**Conceptualization:** Patrick Meyer, Pallab Maity, Andre Burkovski, Christoph Müssel, Hans A. Kestler, Karin Scharffetter-Kochanek.

**Formal analysis:** Hans A. Kestler.

**Funding acquisition:** Hans A. Kestler, Karin Scharffetter-Kochanek.

**Investigation:** Patrick Meyer, Pallab Maity, Julian Schwab, Hans A. Kestler, Karin Scharffetter-Kochanek.

**Methodology:** Andre Burkovski, Karmveer Singh, Filipa F. Ferreira, Linda Krug, Meinhard Wlaschek, Hans A. Kestler.

**Project administration:** Meinhard Wlaschek, Hans A. Kestler, Karin Scharffetter-Kochanek.

**Resources:** Harald J. Maier, Thomas Wirth, Karin Scharffetter-Kochanek.

**Software:** Andre Burkovski, Julian Schwab, Christoph Müssel, Hans A. Kestler.

**Supervision:** Hans A. Kestler, Karin Scharffetter-Kochanek.

**Validation:** Harald J. Maier, Thomas Wirth.

**Writing – original draft:** Patrick Meyer, Andre Burkovski, Hans A. Kestler, Karin Scharffetter-Kochanek.

**Writing – review & editing:** Pallab Maity, Julian Schwab, Christoph Müssel, Hans A. Kestler, Karin Scharffetter-Kochanek.

## References

1. Goldman DP, Cutler D, Rowe JW, Michaud PC, Sullivan J, Peneva D, et al. Substantial health and economic returns from delayed aging may warrant a new focus for medical research. *Health Aff (Millwood)*. 2013; 32(10):1698–705. <https://doi.org/10.1377/hlthaff.2013.0052> PMID: 24101058; PubMed Central PMCID: PMC3938188.
2. Xue W, Zender L, Miething C, Dickins RA, Hernando E, Krizhanovsky V, et al. Senescence and tumour clearance is triggered by p53 restoration in murine liver carcinomas. *Nature*. 2007; 445(7128):656–60. <https://doi.org/10.1038/nature05529> PMID: 17251933.
3. Kuilman T, Michaloglou C, Vredeveld LC, Douma S, van Doorn R, Desmet CJ, et al. Oncogene-induced senescence relayed by an interleukin-dependent inflammatory network. *Cell*. 2008; 133(6):1019–31. <https://doi.org/10.1016/j.cell.2008.03.039> PMID: 18555778.
4. Coppe JP, Patil CK, Rodier F, Sun Y, Munoz DP, Goldstein J, et al. Senescence-associated secretory phenotypes reveal cell-nonautonomous functions of oncogenic RAS and the p53 tumor suppressor. *PLoS Biol*. 2008; 6(12):2853–68. <https://doi.org/10.1371/journal.pbio.0060301> PMID: 19053174; PubMed Central PMCID: PMC2592359.
5. Coppe JP, Patil CK, Rodier F, Krtolica A, Beausejour CM, Parrinello S, et al. A human-like senescence-associated secretory phenotype is conserved in mouse cells dependent on physiological oxygen. *PloS one*. 2010; 5(2):e9188. <https://doi.org/10.1371/journal.pone.0009188> PMID: 20169192; PubMed Central PMCID: PMC2820538.
6. Acosta JC, Banito A, Wuestefeld T, Georgilis A, Janich P, Morton JP, et al. A complex secretory program orchestrated by the inflammasome controls paracrine senescence. *Nature cell biology*. 2013; 15(8):978–90. <https://doi.org/10.1038/ncb2784> PMID: 23770676; PubMed Central PMCID: PMC3732483.

7. Acosta JC, O'Loghlen A, Banito A, Guijarro MV, Augert A, Raguz S, et al. Chemokine signaling via the CXCR2 receptor reinforces senescence. *Cell*. 2008; 133(6):1006–18. <https://doi.org/10.1016/j.cell.2008.03.038> PMID: 18555777.
8. Cohen HJ, Pieper CF, Harris T, Rao KM, Currie MS. The association of plasma IL-6 levels with functional disability in community-dwelling elderly. *J Gerontol A Biol Sci Med Sci*. 1997; 52(4):M201–8. PMID: 9224431.
9. Rodier F, Coppe JP, Patil CK, Hoeijmakers WA, Munoz DP, Raza SR, et al. Persistent DNA damage signalling triggers senescence-associated inflammatory cytokine secretion. *Nature cell biology*. 2009; 11(8):973–9. <https://doi.org/10.1038/ncb1909> PMID: 19597488; PubMed Central PMCID: PMC2743561.
10. Davidson EH, Erwin DH. Gene regulatory networks and the evolution of animal body plans. *Science*. 2006; 311(5762):796–800. <https://doi.org/10.1126/science.1113832> PMID: 16469913.
11. Kestler HA, Wawra C, Kracher B, Kühl M. Network modeling of signal transduction: establishing the global view. *Bioessays*. 2008; 30(11–12):1110–25. <https://doi.org/10.1002/bies.20834> PMID: 18937364.
12. Naldi A, Monteiro PT, Müssel C, Consortium for Logical M, Tools, Kestler HA, et al. Cooperative development of logical modelling standards and tools with CoLoMoTo. *Bioinformatics*. 2015; 31(7):1154–9. <https://doi.org/10.1093/bioinformatics/btv013> PMID: 25619997.
13. Shmulevich I, Dougherty ER. *Genomic Signal Processing*: Princeton University Press; 2007.
14. de Jong H. Modeling and simulation of genetic regulatory systems: a literature review. *J Comput Biol*. 2002; 9(1):67–103. <https://doi.org/10.1089/10665270252833208> PMID: 11911796.
15. Kauffman S. Homeostasis and differentiation in random genetic control networks. *Nature*. 1969; 224(5215):177–8. PMID: 5343519.
16. Le Novère N. Quantitative and logic modelling of molecular and gene networks. *Nat Rev Genet*. 2015; 16(3):146–58. <https://doi.org/10.1038/nrg3885> PMID: 25645874; PubMed Central PMCID: PMCPMC4604653.
17. Fisher J, Henzinger TA. Executable cell biology. *Nature biotechnology*. 2007; 25(11):1239–49. <https://doi.org/10.1038/nbt1356> PMID: 17989686.
18. Harvey I, Bossomaier T. Time Out of Joint: Attractors in Asynchronous Random Boolean Networks. In: Husbands P, Harvey I, editors. *Proceedings of the Fourth European Artificial Life Conference*: MIT Press; 1997. p. 67–75.
19. Klarner H, Bockmayr A, Siebert H. Computing Symbolic Steady States of Boolean Networks. In: Wąs J, Sirakoulis GC, Bandini S, editors. *Cellular Automata: 11th International Conference on Cellular Automata for Research and Industry, ACRI 2014, Krakow, Poland, September 22–25, 2014 Proceedings*. Cham: Springer International Publishing; 2014. p. 561–70.
20. Zañudo JGT, Albert R. An effective network reduction approach to find the dynamical repertoire of discrete dynamic networks. *Chaos: An Interdisciplinary Journal of Nonlinear Science*. 2013; 23(2):025111. <https://doi.org/10.1063/1.4809777> PMID: 23822509.
21. Dahlhaus M, Burkovski A, Hertwig F, Mussel C, Volland R, Fischer M, et al. Boolean modeling identifies Greatwall/MASTL as an important regulator in the AURKA network of neuroblastoma. *Cancer letters*. 2016; 371(1):79–89. <https://doi.org/10.1016/j.canlet.2015.11.025> PMID: 26616283.
22. MacLean D, Studholme DJ. A Boolean model of the *Pseudomonas syringae* hrp regulon predicts a tightly regulated system. *PLoS one*. 2010; 5(2):e9101. <https://doi.org/10.1371/journal.pone.0009101> PMID: 20169167; PubMed Central PMCID: PMC2821412.
23. Moignard V, Woodhouse S, Haghverdi L, Lilly AJ, Tanaka Y, Wilkinson AC, et al. Decoding the regulatory network of early blood development from single-cell gene expression measurements. *Nature biotechnology*. 2015; 33(3):269–76. <https://doi.org/10.1038/nbt.3154> PMID: 25664528; PubMed Central PMCID: PMCPMC4374163.
24. Herrmann F, Gross A, Zhou D, Kestler HA, Kühl M. A boolean model of the cardiac gene regulatory network determining first and second heart field identity. *PLoS one*. 2012; 7(10):e46798. <https://doi.org/10.1371/journal.pone.0046798> PMID: 23056457; PubMed Central PMCID: PMC3462786.
25. Kestler HA, Kuhl M. From individual Wnt pathways towards a Wnt signalling network. *Philosophical transactions of the Royal Society of London Series B, Biological sciences*. 2008; 363(1495):1333–47. <https://doi.org/10.1098/rstb.2007.2251> PMID: 18192173; PubMed Central PMCID: PMCPMC2610122.
26. Feist AM, Herrgard MJ, Thiele I, Reed JL, Palsson BO. Reconstruction of biochemical networks in microorganisms. *Nat Rev Microbiol*. 2009; 7(2):129–43. <https://doi.org/10.1038/nrmicro1949> PMID: 19116616; PubMed Central PMCID: PMCPMC3119670.

27. Saadatpour A, Albert R, Reluga TC. A Reduction Method for Boolean Network Models Proven to Conserve Attractors. *SIAM Journal on Applied Dynamical Systems*. 2013; 12(4):1997–2011. <https://doi.org/10.1137/13090537x>
28. Veliz-Cuba A. Reduction of Boolean network models. *Journal of theoretical biology*. 2011; 289:167–72. <https://doi.org/10.1016/j.jtbi.2011.08.042> PMID: 21907211.
29. Hiscott J, Marois J, Garoufalidis J, D'Addario M, Roulston A, Kwan I, et al. Characterization of a functional NF-kappa B site in the human interleukin 1 beta promoter: evidence for a positive autoregulatory loop. *Molecular and cellular biology*. 1993; 13(10):6231–40. PMID: 8413223; PubMed Central PMCID: PMC364682.
30. Mori N, Prager D. Transactivation of the interleukin-1alpha promoter by human T-cell leukemia virus type I and type II Tax proteins. *Blood*. 1996; 87(8):3410–7. PMID: 8605359.
31. Holtmann H, Winzen R, Holland P, Eickemeier S, Hoffmann E, Wallach D, et al. Induction of interleukin-8 synthesis integrates effects on transcription and mRNA degradation from at least three different cytokine- or stress-activated signal transduction pathways. *Molecular and cellular biology*. 1999; 19(10):6742–53. PMID: 10490613; PubMed Central PMCID: PMC84667.
32. Libermann TA, Baltimore D. Activation of interleukin-6 gene expression through the NF-kappa B transcription factor. *Molecular and cellular biology*. 1990; 10(5):2327–34. PMID: 2183031; PubMed Central PMCID: PMC360580.
33. Son YH, Jeong YT, Lee KA, Choi KH, Kim SM, Rhim BY, et al. Roles of MAPK and NF-kappaB in interleukin-6 induction by lipopolysaccharide in vascular smooth muscle cells. *Journal of cardiovascular pharmacology*. 2008; 51(1):71–7. <https://doi.org/10.1097/FJC.0b013e31815bd23d> PMID: 18209571.
34. Park GY, Le S, Park KH, Le CT, Kim YW, Han SK, et al. Anti-inflammatory effect of adenovirus-mediated IkappaBalphα overexpression in respiratory epithelial cells. *The European respiratory journal*. 2001; 18(5):801–9. PMID: 11757631.
35. Schmidt-Supplian M, Bloch W, Courtois G, Addicks K, Israel A, Rajewsky K, et al. NEMO/IKK gamma-deficient mice model incontinentia pigmenti. *Molecular cell*. 2000; 5(6):981–92. PMID: 10911992.
36. Salminen A, Suuronen T, Huuskonen J, Kaarniranta K. NEMO shuttle: a link between DNA damage and NF-kappaB activation in progeroid syndromes? *Biochemical and biophysical research communications*. 2008; 367(4):715–8. <https://doi.org/10.1016/j.bbrc.2007.11.189> PMID: 18201555.
37. Zurgil U, Ben-Ari A, Atias K, Isakov N, Apte R, Livneh E. PKCeta promotes senescence induced by oxidative stress and chemotherapy. *Cell death & disease*. 2014; 5:e1531. <https://doi.org/10.1038/cddis.2014.481> PMID: 25412309; PubMed Central PMCID: PMCPMC4260739.
38. Dyson N. The regulation of E2F by pRB-family proteins. *Genes & development*. 1998; 12(15):2245–62. PMID: 9694791.
39. Salminen A, Kauppinen A, Kaarniranta K. Emerging role of NF-kappaB signaling in the induction of senescence-associated secretory phenotype (SASP). *Cellular signalling*. 2012; 24(4):835–45. <https://doi.org/10.1016/j.cellsig.2011.12.006> PMID: 22182507.
40. Sebban H, Yamaoka S, Courtois G. Posttranslational modifications of NEMO and its partners in NF-kappaB signaling. *Trends Cell Biol*. 2006; 16(11):569–77. <https://doi.org/10.1016/j.tcb.2006.09.004> PMID: 16987664.
41. Israel A. The IKK complex, a central regulator of NF-kappaB activation. *Cold Spring Harbor perspectives in biology*. 2010; 2(3):a000158. <https://doi.org/10.1101/cshperspect.a000158> PMID: 20300203; PubMed Central PMCID: PMCPMC2829958.
42. Di Micco R, Furnagalli M, Cicalese A, Piccinini S, Gasparini P, Luise C, et al. Oncogene-induced senescence is a DNA damage response triggered by DNA hyper-replication. *Nature*. 2006; 444(7119):638–42. <https://doi.org/10.1038/nature05327> PMID: 17136094.
43. Gensler HL, Bernstein H. DNA damage as the primary cause of aging. *Q Rev Biol*. 1981; 56(3):279–303. PMID: 7031747.
44. Holmes GE, Bernstein C, Bernstein H. Oxidative and other DNA damages as the basis of aging: a review. *Mutat Res*. 1992; 275(3–6):305–15. PMID: 1383772.
45. Badache A, Hynes NE. Interleukin 6 inhibits proliferation and, in cooperation with an epidermal growth factor receptor autocrine loop, increases migration of T47D breast cancer cells. *Cancer research*. 2001; 61(1):383–91. PMID: 11196191.
46. Coppe JP, Desprez PY, Krötzka A, Campisi J. The senescence-associated secretory phenotype: the dark side of tumor suppression. *Annu Rev Pathol*. 2010; 5:99–118. <https://doi.org/10.1146/annurev-pathol-121808-102144> PMID: 20078217; PubMed Central PMCID: PMCPMC4166495.

47. Krizhanovsky V, Yon M, Dickins RA, Hearn S, Simon J, Miething C, et al. Senescence of activated stellate cells limits liver fibrosis. *Cell.* 2008; 134(4):657–67. <https://doi.org/10.1016/j.cell.2008.06.049> PMID: 18724938; PubMed Central PMCID: PMC3073300.
48. Lee JK, Bettencourt R, Brenner D, Le TA, Barrett-Connor E, Loomba R. Association between serum interleukin-6 concentrations and mortality in older adults: the Rancho Bernardo study. *PloS one.* 2012; 7(4):e34218. <https://doi.org/10.1371/journal.pone.0034218> PMID: 22514624; PubMed Central PMCID: PMC325993.
49. Habineza Ndikuyeze G, Gaurnier-Hausser A, Patel R, Baldwin AS, May MJ, Flood P, et al. A phase I clinical trial of systemically delivered NEMO binding domain peptide in dogs with spontaneous activated B-cell like diffuse large B-cell lymphoma. *PloS one.* 2014; 9(5):e95404. <https://doi.org/10.1371/journal.pone.0095404> PMID: 24798348; PubMed Central PMCID: PMC4010398.
50. Dai S, Hirayama T, Abbas S, Abu-Amer Y. The IkappaB kinase (IKK) inhibitor, NEMO-binding domain peptide, blocks osteoclastogenesis and bone erosion in inflammatory arthritis. *The Journal of biological chemistry.* 2004; 279(36):37219–22. <https://doi.org/10.1074/jbc.C400258200> PMID: 15252035.
51. Zheng B, Zhang Z, Black CM, de Crombrugghe B, Denton CP. Ligand-dependent genetic recombination in fibroblasts: a potentially powerful technique for investigating gene function in fibrosis. *The American journal of pathology.* 2002; 160(5):1609–17. [https://doi.org/10.1016/S0002-9440\(10\)61108-X](https://doi.org/10.1016/S0002-9440(10)61108-X) PMID: 12000713; PubMed Central PMCID: PMC1850857.
52. Treiber N, Maity P, Singh K, Kohn M, Keist AF, Ferchiu F, et al. Accelerated aging phenotype in mice with conditional deficiency for mitochondrial superoxide dismutase in the connective tissue. *Aging cell.* 2011; 10(2):239–54. <https://doi.org/10.1111/j.1474-9726.2010.00658.x> PMID: 21108731.
53. Wang H, Bian X, Xia L, Ding X, Muller R, Zhang Y, et al. Improved seamless mutagenesis by recombinering using ccdB for counterselection. *Nucleic acids research.* 2014; 42(5):e37. <https://doi.org/10.1093/nar/gkt1339> PMID: 24369425; PubMed Central PMCID: PMC3950717.
54. Singh K, Maity P, Krug L, Meyer P, Treiber N, Lucas T, et al. Superoxide anion radicals induce IGF-1 resistance through concomitant activation of PTP1B and PTEN. *EMBO Mol Med.* 2015; 7(1):59–77. <https://doi.org/10.1525/emmm.201404082> PMID: 25520316; PubMed Central PMCID: PMC4309668.
55. Zañudo JG, Albert R. Cell fate reprogramming by control of intracellular network dynamics. *PLoS computational biology.* 2015; 11(4):e1004193. <https://doi.org/10.1371/journal.pcbi.1004193> PMID: 25849586; PubMed Central PMCID: PMC4388852.
56. Müssel C, Hopfensitz M, Kestler HA. BoolNet—an R package for generation, reconstruction and analysis of Boolean networks. *Bioinformatics.* 2010; 26(10):1378–80. <https://doi.org/10.1093/bioinformatics/btq124> PMID: 20378558.
57. Sancar A, Lindsey-Boltz LA, Unsal-Kacmaz K, Linn S. Molecular mechanisms of mammalian DNA repair and the DNA damage checkpoints. *Annual review of biochemistry.* 2004; 73:39–85. <https://doi.org/10.1146/annurev.biochem.73.011303.073723> PMID: 15189136.
58. Shiloh Y. ATM and related protein kinases: safeguarding genome integrity. *Nature reviews Cancer.* 2003; 3(3):155–68. <https://doi.org/10.1038/nrc1011> PMID: 12612651.
59. Smith J, Tho LM, Xu N, Gillespie DA. The ATM-Chk2 and ATR-Chk1 pathways in DNA damage signaling and cancer. *Advances in cancer research.* 2010; 108:73–112. <https://doi.org/10.1016/B978-0-12-380888-2.00003-0> PMID: 21034966.
60. Falck J, Mailand N, Syljuasen RG, Bartek J, Lukas J. The ATM-Chk2-Cdc25A checkpoint pathway guards against radioresistant DNA synthesis. *Nature.* 2001; 410(6830):842–7. <https://doi.org/10.1038/35071124> PMID: 11298456.
61. Zhan Q, Fan S, Smith ML, Bae I, Yu K, Alamo I Jr, et al. Abrogation of p53 function affects gadd gene responses to DNA base-damaging agents and starvation. *DNA and cell biology.* 1996; 15(10):805–15. <https://doi.org/10.1089/dna.1996.15.805> PMID: 8892753.
62. Appella E, Anderson CW. Post-translational modifications and activation of p53 by genotoxic stresses. *European journal of biochemistry / FEBS.* 2001; 268(10):2764–72. PMID: 11358490.
63. Hirao A, Kong YY, Matsuoka S, Wakeham A, Ruland J, Yoshida H, et al. DNA damage-induced activation of p53 by the checkpoint kinase Chk2. *Science.* 2000; 287(5459):1824–7. PMID: 10710310.
64. Cheng Q, Chen L, Li Z, Lane WS, Chen J. ATM activates p53 by regulating MDM2 oligomerization and E3 processivity. *The EMBO journal.* 2009; 28(24):3857–67. <https://doi.org/10.1038/emboj.2009.294> PMID: 19816404; PubMed Central PMCID: PMC2797053.
65. Jones SN, Roe AE, Donehower LA, Bradley A. Rescue of embryonic lethality in Mdm2-deficient mice by absence of p53. *Nature.* 1995; 378(6553):206–8. <https://doi.org/10.1038/378206a0> PMID: 7477327.

66. Ke Q, Costa M. Hypoxia-inducible factor-1 (HIF-1). *Molecular pharmacology*. 2006; 70(5):1469–80. <https://doi.org/10.1124/mol.106.027029> PMID: 16887934.
67. Blagosklonny MV, An WG, Romanova LY, Trepel J, Fojo T, Neckers L. p53 inhibits hypoxia-inducible factor-stimulated transcription. *The Journal of biological chemistry*. 1998; 273(20):11995–8. PMID: 9575138.
68. Xiong Y, Hannon GJ, Zhang H, Casso D, Kobayashi R, Beach D. p21 is a universal inhibitor of cyclin kinases. *Nature*. 1993; 366(6456):701–4. <https://doi.org/10.1038/366701a0> PMID: 8259214.
69. Herold S, Wanzel M, Beugler V, Frohme C, Beul D, Hillukkala T, et al. Negative regulation of the mammalian UV response by Myc through association with Miz-1. *Molecular cell*. 2002; 10(3):509–21. PMID: 12408820.
70. Brugarolas J, Moberg K, Boyd SD, Taya Y, Jacks T, Lees JA. Inhibition of cyclin-dependent kinase 2 by p21 is necessary for retinoblastoma protein-mediated G1 arrest after gamma-irradiation. *Proceedings of the National Academy of Sciences of the United States of America*. 1999; 96(3):1002–7. PMID: 9927683; PubMed Central PMCID: PMC15340.
71. Grafstrom RH, Pan W, Hoess RH. Defining the substrate specificity of cdk4 kinase-cyclin D1 complex. *Carcinogenesis*. 1999; 20(2):193–8. PMID: 10069453.
72. Weinberg RA. The retinoblastoma protein and cell cycle control. *Cell*. 1995; 81(3):323–30. PMID: 7736585.
73. Barak Y, Juven T, Haffner R, Oren M. mdm2 expression is induced by wild type p53 activity. *The EMBO journal*. 1993; 12(2):461–8. PMID: 8440237; PubMed Central PMCID: PMC413229.
74. Moll UM, Petrenko O. The MDM2-p53 interaction. *Molecular cancer research: MCR*. 2003; 1(14):1001–8. PMID: 14707283.
75. Shapiro GI, Edwards CD, Ewen ME, Rollins BJ. p16INK4A participates in a G1 arrest checkpoint in response to DNA damage. *Molecular and cellular biology*. 1998; 18(1):378–87. PMID: 9418885; PubMed Central PMCID: PMC121508.
76. Wuerzberger-Davis SM, Nakamura Y, Seufzer BJ, Miyamoto S. NF-kappaB activation by combinations of NEMO SUMOylation and ATM activation stresses in the absence of DNA damage. *Oncogene*. 2007; 26(5):641–51. <https://doi.org/10.1038/sj.onc.1209815> PMID: 16862178.
77. Yang Y, Xia F, Hermance N, Mabb A, Simonson S, Morrissey S, et al. A cytosolic ATM/NEMO/RIP1 complex recruits TAK1 to mediate the NF-kappaB and p38 mitogen-activated protein kinase (MAPK)/MAPK-activated protein 2 responses to DNA damage. *Molecular and cellular biology*. 2011; 31(14):2774–86. <https://doi.org/10.1128/MCB.01139-10> PMID: 21606198; PubMed Central PMCID: PMC3133388.
78. Wu ZH, Wong ET, Shi Y, Niu J, Chen Z, Miyamoto S, et al. ATM- and NEMO-dependent ELKS ubiquitination coordinates TAK1-mediated IKK activation in response to genotoxic stress. *Molecular cell*. 2010; 40(1):75–86. <https://doi.org/10.1016/j.molcel.2010.09.010> PMID: 20932476; PubMed Central PMCID: PMC3048026.
79. Ling L, Cao Z, Goeddel DV. NF-kappaB-inducing kinase activates IKK-alpha by phosphorylation of Ser-176. *Proceedings of the National Academy of Sciences of the United States of America*. 1998; 95(7):3792–7. PMID: 9520446; PubMed Central PMCID: PMC19916.
80. Bai D, Ueno L, Vogt PK. Akt-mediated regulation of NF kappaB and the essentialness of NF kappaB for the oncogenicity of PI3K and Akt. *International journal of cancer Journal international du cancer*. 2009; 125(12):2863–70. <https://doi.org/10.1002/ijc.24748> PMID: 19609947; PubMed Central PMCID: PMCPMC2767458.
81. Sun SC, Ganchi PA, Ballard DW, Greene WC. NF-kappa B controls expression of inhibitor I kappa B alpha: evidence for an inducible autoregulatory pathway. *Science*. 1993; 259(5103):1912–5. PMID: 8096091.
82. Zandi E, Rothwarf DM, Delhase M, Hayakawa M, Karin M. The IkappaB kinase complex (IKK) contains two kinase subunits, IKKalpha and IKKbeta, necessary for IkappaB phosphorylation and NF-kappaB activation. *Cell*. 1997; 91(2):243–52. PMID: 9346241.
83. Hinz M, Scheidereit C. The IkappaB kinase complex in NF-kappaB regulation and beyond. *EMBO reports*. 2014; 15(1):46–61. <https://doi.org/10.1002/embr.201337983> PMID: 24375677; PubMed Central PMCID: PMCPMC4303448.
84. Weber A, Wasiliew P, Kracht M. Interleukin-1 (IL-1) pathway. *Science signaling*. 2010; 3(105):cm1. <https://doi.org/10.1126/scisignal.3105cm1> PMID: 20086235.
85. Kawagoe T, Sato S, Matsushita K, Kato H, Matsui K, Kumagai Y, et al. Sequential control of Toll-like receptor-dependent responses by IRAK1 and IRAK2. *Nature immunology*. 2008; 9(6):684–91. <https://doi.org/10.1038/ni.1606> PMID: 18438411.

86. Li S, Strelow A, Fontana EJ, Wesche H. IRAK-4: a novel member of the IRAK family with the properties of an IRAK-kinase. *Proceedings of the National Academy of Sciences of the United States of America*. 2002; 99(8):5567–72. <https://doi.org/10.1073/pnas.082100399> PMID: 11960013; PubMed Central PMCID: PMC122810.
87. Wesche H, Henzel WJ, Shillinglaw W, Li S, Cao Z. MyD88: an adapter that recruits IRAK to the IL-1 receptor complex. *Immunity*. 1997; 7(6):837–47. PMID: 9430229.
88. Yamasaki K, Taga T, Hirata Y, Yawata H, Kawanishi Y, Seed B, et al. Cloning and expression of the human interleukin-6 (BSF-2/IFN beta 2) receptor. *Science*. 1988; 241(4867):825–8. PMID: 3136546.
89. Yao J, Kim TW, Qin J, Jiang Z, Qian Y, Xiao H, et al. Interleukin-1 (IL-1)-induced TAK1-dependent Versus MEKK3-dependent NFκappaB activation pathways bifurcate at IL-1 receptor-associated kinase modification. *The Journal of biological chemistry*. 2007; 282(9):6075–89. <https://doi.org/10.1074/jbc.M609039200> PMID: 17197697.
90. Kanayama A, Seth RB, Sun L, Ea CK, Hong M, Shaito A, et al. TAB2 and TAB3 activate the NF-κappaB pathway through binding to polyubiquitin chains. *Molecular cell*. 2004; 15(4):535–48. <https://doi.org/10.1016/j.molcel.2004.08.008> PMID: 15327770.
91. Ninomiya-Tsuji J, Kishimoto K, Hiyama A, Inoue J, Cao Z, Matsumoto K. The kinase TAK1 can activate the NIK-I kappaB as well as the MAP kinase cascade in the IL-1 signalling pathway. *Nature*. 1999; 398(6724):252–6. <https://doi.org/10.1038/18465> PMID: 10094049.
92. Wang C, Deng L, Hong M, Akkaraju GR, Inoue J, Chen ZJ. TAK1 is a ubiquitin-dependent kinase of MKK and IKK. *Nature*. 2001; 412(6844):346–51. <https://doi.org/10.1038/35085597> PMID: 11460167.
93. Hammaker DR, Boyle DL, Chabaud-Riou M, Firestein GS. Regulation of c-Jun N-terminal kinase by MEKK-2 and mitogen-activated protein kinase kinases in rheumatoid arthritis. *Journal of immunology*. 2004; 172(3):1612–8. PMID: 14734742.
94. Finch A, Holland P, Cooper J, Saklatvala J, Kracht M. Selective activation of JNK/SAPK by interleukin-1 in rabbit liver is mediated by MKK7. *FEBS letters*. 1997; 418(1–2):144–8. PMID: 9414114.
95. Tournier C, Dong C, Turner TK, Jones SN, Flavell RA, Davis RJ. MKK7 is an essential component of the JNK signal transduction pathway activated by proinflammatory cytokines. *Genes & development*. 2001; 15(11):1419–26. <https://doi.org/10.1101/gad.888501> PMID: 11390361; PubMed Central PMCID: PMC312702.
96. Kristiansen M, Hughes R, Patel P, Jacques TS, Clark AR, Ham J. Mkp1 is a c-Jun target gene that antagonizes JNK-dependent apoptosis in sympathetic neurons. *The Journal of neuroscience: the official journal of the Society for Neuroscience*. 2010; 30(32):10820–32. <https://doi.org/10.1523/JNEUROSCI.2824-10.2010> PMID: 20702711; PubMed Central PMCID: PMC3044878.
97. Inoue T, Hammaker D, Boyle DL, Firestein GS. Regulation of p38 MAPK by MAPK kinases 3 and 6 in fibroblast-like synoviocytes. *Journal of immunology*. 2005; 174(7):4301–6. PMID: 15778394.
98. Kiemer AK, Weber NC, Furst R, Bildner N, Kulhanek-Heinze S, Vollmar AM. Inhibition of p38 MAPK activation via induction of MKP-1: atrial natriuretic peptide reduces TNF-alpha-induced actin polymerization and endothelial permeability. *Circulation research*. 2002; 90(8):874–81. PMID: 11988488.
99. van Dam H, Wilhelm D, Herr I, Steffen A, Herrlich P, Angel P. ATF-2 is preferentially activated by stress-activated protein kinases to mediate c-jun induction in response to genotoxic agents. *The EMBO journal*. 1995; 14(8):1798–811. PMID: 7737130; PubMed Central PMCID: PMC398273.
100. Wadgaonkar R, Pierce JW, Somnay K, Damico RL, Crow MT, Collins T, et al. Regulation of c-Jun N-terminal kinase and p38 kinase pathways in endothelial cells. *American journal of respiratory cell and molecular biology*. 2004; 31(4):423–31. <https://doi.org/10.1165/rcmb.2003-0384OC> PMID: 15231489.
101. Minden A, Lin A, Smeal T, Derijard B, Cobb M, Davis R, et al. c-Jun N-terminal phosphorylation correlates with activation of the JNK subgroup but not the ERK subgroup of mitogen-activated protein kinases. *Molecular and cellular biology*. 1994; 14(10):6683–8. PMID: 7935387; PubMed Central PMCID: PMC359198.
102. Pulverer BJ, Kyriakis JM, Avruch J, Nikolakaki E, Woodgett JR. Phosphorylation of c-jun mediated by MAP kinases. *Nature*. 1991; 353(6345):670–4. <https://doi.org/10.1038/353670a0> PMID: 1922387.
103. Hanlon M, Bundy LM, Sealy L. C/EBP beta and Elk-1 synergistically transactivate the c-fos serum response element. *BMC cell biology*. 2000; 1:2. <https://doi.org/10.1186/1471-2121-1-2> PMID: 11151091; PubMed Central PMCID: PMC29063.
104. Silvers AL, Bachelor MA, Bowden GT. The role of JNK and p38 MAPK activities in UVA-induced signaling pathways leading to AP-1 activation and c-Fos expression. *Neoplasia*. 2003; 5(4):319–29. [https://doi.org/10.1016/S1476-5586\(03\)80025-8](https://doi.org/10.1016/S1476-5586(03)80025-8) PMID: 14511403; PubMed Central PMCID: PMC1502419.
105. Babu GJ, Lalli MJ, Sussman MA, Sadoshima J, Periasamy M. Phosphorylation of elk-1 by MEK/ERK pathway is necessary for c-fos gene activation during cardiac myocyte hypertrophy. *Journal of*

- molecular and cellular cardiology. 2000; 32(8):1447–57. <https://doi.org/10.1006/jmcc.2000.1185> PMID: 10900171.
106. Cavigelli M, Dolfi F, Claret FX, Karin M. Induction of c-fos expression through JNK-mediated TCF/Elk-1 phosphorylation. *The EMBO journal*. 1995; 14(23):5957–64. PMID: 8846788; PubMed Central PMCID: PMC394715.
  107. Yang E, Lerner L, Besser D, Darnell JE Jr. Independent and cooperative activation of chromosomal c-fos promoter by STAT3. *The Journal of biological chemistry*. 2003; 278(18):15794–9. <https://doi.org/10.1074/jbc.M213073200> PMID: 12600988.
  108. Angel P, Karin M. The role of Jun, Fos and the AP-1 complex in cell-proliferation and transformation. *Biochimica et biophysica acta*. 1991; 1072(2–3):129–57. PMID: 1751545.
  109. Casals-Casas C, Alvarez E, Serra M, de la Torre C, Farrera C, Sanchez-Tillo E, et al. CREB and AP-1 activation regulates MKP-1 induction by LPS or M-CSF and their kinetics correlate with macrophage activation versus proliferation. *European journal of immunology*. 2009; 39(7):1902–13. <https://doi.org/10.1002/eji.200839037> PMID: 19585511.
  110. Sanchez-Tillo E, Comalada M, Xaus J, Farrera C, Valledor AF, Caelles C, et al. JNK1 is required for the induction of Mkp1 expression in macrophages during proliferation and lipopolysaccharide-dependent activation. *The Journal of biological chemistry*. 2007; 282(17):12566–73. <https://doi.org/10.1074/jbc.M609662200> PMID: 17337450.
  111. Kang HB, Kim YE, Kwon HJ, Sok DE, Lee Y. Enhancement of NF-kappaB expression and activity upon differentiation of human embryonic stem cell line SNUhES3. *Stem cells and development*. 2007; 16(4):615–23. <https://doi.org/10.1089/scd.2007.0014> PMID: 17784835.
  112. Kunsch C, Rosen CA. NF-kappa B subunit-specific regulation of the interleukin-8 promoter. *Molecular and cellular biology*. 1993; 13(10):6137–46. PMID: 8413215; PubMed Central PMCID: PMC364673.
  113. Neff L, Zeisel M, Druet V, Takeda K, Klein JP, Sibilia J, et al. ERK 1/2- and JNKs-dependent synthesis of interleukins 6 and 8 by fibroblast-like synoviocytes stimulated with protein I/II, a modulin from oral streptococci, requires focal adhesion kinase. *The Journal of biological chemistry*. 2003; 278(30):27721–8. <https://doi.org/10.1074/jbc.M212065200> PMID: 12761229.
  114. Neff L, Zeisel M, Sibilia J, Scholler-Guinard M, Klein JP, Wachsmann D. NF-kappaB and the MAP kinases/AP-1 pathways are both involved in interleukin-6 and interleukin-8 expression in fibroblast-like synoviocytes stimulated by protein I/II, a modulin from oral streptococci. *Cellular microbiology*. 2001; 3(10):703–12. PMID: 11580755.
  115. Akira S, Isshiki H, Sugita T, Tanabe O, Kinoshita S, Nishio Y, et al. A nuclear factor for IL-6 expression (NF-IL6) is a member of a C/EBP family. *The EMBO journal*. 1990; 9(6):1897–906. PMID: 2112087; PubMed Central PMCID: PMC551896.
  116. Heinrich PC, Behrmann I, Haan S, Hermanns HM, Muller-Newen G, Schaper F. Principles of interleukin (IL)-6-type cytokine signalling and its regulation. *The Biochemical journal*. 2003; 374(Pt 1):1–20. <https://doi.org/10.1042/BJ20030407> PMID: 12773095; PubMed Central PMCID: PMC1223585.
  117. Heinrich PC, Behrmann I, Muller-Newen G, Schaper F, Graeve L. Interleukin-6-type cytokine signalling through the gp130/Jak/STAT pathway. *The Biochemical journal*. 1998; 334 (Pt 2):297–314. PMID: 9716487; PubMed Central PMCID: PMC1219691.
  118. Murakami M, Hibi M, Nakagawa N, Nakagawa T, Yasukawa K, Yamanishi K, et al. IL-6-induced homodimerization of gp130 and associated activation of a tyrosine kinase. *Science*. 1993; 260(5115):1808–10. PMID: 8511589.
  119. Harrison DA. The Jak/STAT pathway. *Cold Spring Harbor perspectives in biology*. 2012; 4(3). <https://doi.org/10.1101/cshperspect.a011205> PMID: 22383755; PubMed Central PMCID: PMC3282412.
  120. Kershaw NJ, Murphy JM, Liau NP, Varghese LN, Laktyushin A, Whitlock EL, et al. SOCS3 binds specific receptor-JAK complexes to control cytokine signaling by direct kinase inhibition. *Nature structural & molecular biology*. 2013; 20(4):469–76. <https://doi.org/10.1038/nsmb.2519> PMID: 23454976; PubMed Central PMCID: PMC3618588.
  121. Blanco-Aparicio C, Renner O, Leal JF, Carnero A. PTEN, more than the AKT pathway. *Carcinogenesis*. 2007; 28(7):1379–86. <https://doi.org/10.1093/carcin/bgm052> PMID: 17341655.
  122. Kandel ES, Hay N. The regulation and activities of the multifunctional serine/threonine kinase Akt/PKB. *Experimental cell research*. 1999; 253(1):210–29. <https://doi.org/10.1006/excr.1999.4690> PMID: 10579924.
  123. Hahn-Windgassen A, Nogueira V, Chen CC, Skeen JE, Sonenberg N, Hay N. Akt activates the mammalian target of rapamycin by regulating cellular ATP level and AMPK activity. *The Journal of biological chemistry*. 2005; 280(37):32081–9. <https://doi.org/10.1074/jbc.M502876200> PMID: 16027121.
  124. Yu H, Pardoll D, Jove R. STATs in cancer inflammation and immunity: a leading role for STAT3. *Nature reviews Cancer*. 2009; 9(11):798–809. <https://doi.org/10.1038/nrc2734> PMID: 19851315.

125. Giordano V, De Falco G, Chiari R, Quinto I, Pelicci PG, Bartholomew L, et al. Shc mediates IL-6 signaling by interacting with gp130 and Jak2 kinase. *Journal of immunology*. 1997; 158(9):4097–103. PMID: [9126968](#).
126. Roberts PJ, Der CJ. Targeting the Raf-MEK-ERK mitogen-activated protein kinase cascade for the treatment of cancer. *Oncogene*. 2007; 26(22):3291–310. <https://doi.org/10.1038/sj.onc.1210422> PMID: [17496923](#).
127. Liu H, Yao S, Dann SM, Qin H, Elson CO, Cong Y. ERK differentially regulates Th17- and Treg-cell development and contributes to the pathogenesis of colitis. *European journal of immunology*. 2013; 43(7):1716–26. <https://doi.org/10.1002/eji.201242889> PMID: [23620016](#).
128. Cruzalegui FH, Cano E, Treisman R. ERK activation induces phosphorylation of Elk-1 at multiple S/T-P motifs to high stoichiometry. *Oncogene*. 1999; 18(56):7948–57. <https://doi.org/10.1038/sj.onc.1203362> PMID: [10637505](#).
129. Yokogami K, Wakisaka S, Avruch J, Reeves SA. Serine phosphorylation and maximal activation of STAT3 during CNTF signaling is mediated by the rapamycin target mTOR. *Current biology: CB*. 2000; 10(1):47–50. PMID: [10660304](#).
130. Schuringa JJ, Timmer H, Luttkhuizen D, Vellenga E, Kruijer W. c-Jun and c-Fos cooperate with STAT3 in IL-6-induced transactivation of the IL-6 response element (IRE). *Cytokine*. 2001; 14(2):78–87. <https://doi.org/10.1006/cyto.2001.0856> PMID: [11356008](#).